CASE FILE
COPY

CAVITATION IN LIQUID CRYOGENS

IV - Combined Correlations for Venturi, Hydrofoil, Ogives, and Pumps
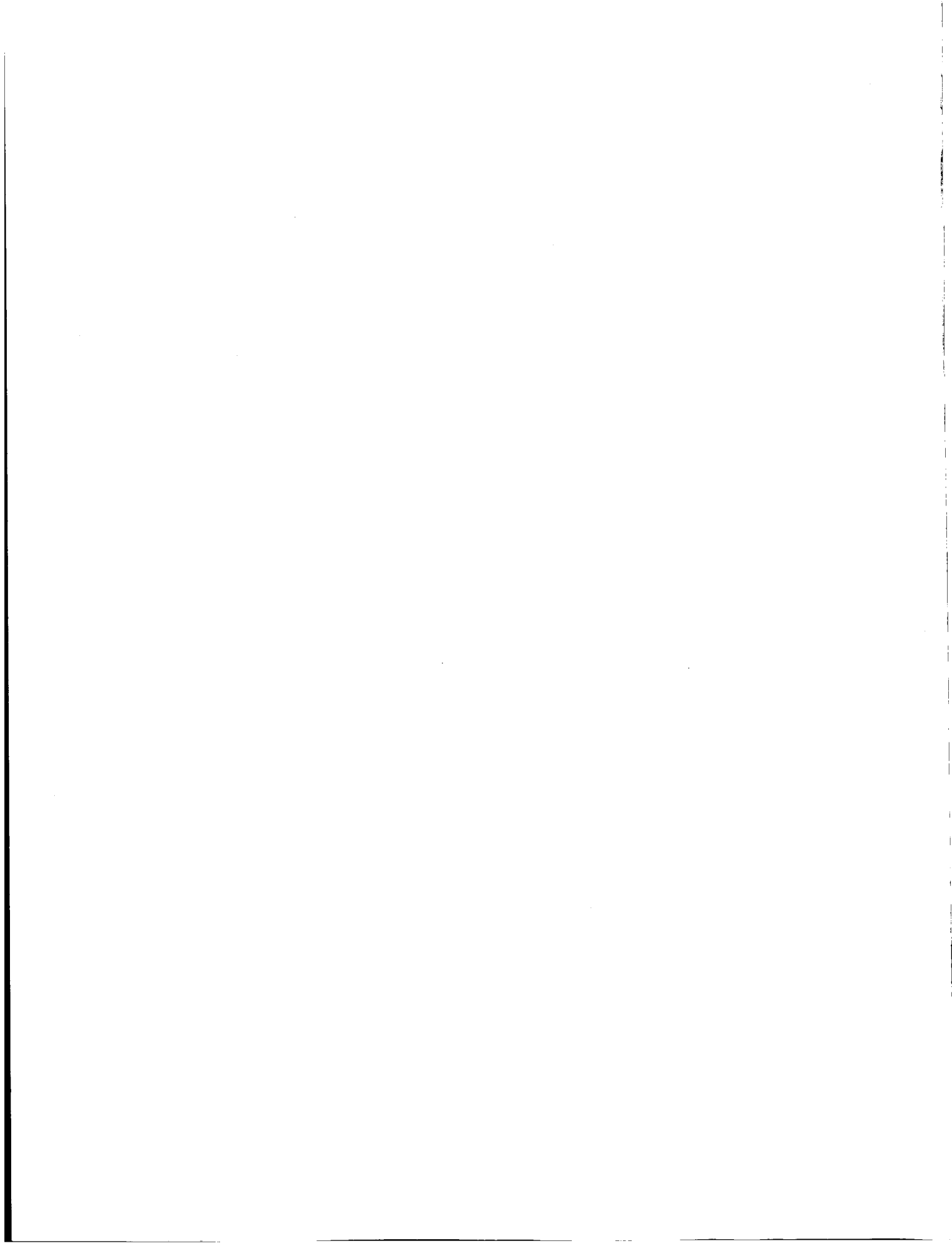
by J. Hord

Prepared by
NATIONAL BUREAU OF STANDARDS
Boulder, Colo. 80302
for Lewis Research Center

NATIONAL AERONAUTICS AND SPACE ADMINISTRATION • WASHINGTON, D. C. • OCTOBER 1974

1. Report No. NASA CR-2448	2. Government Accession No.	3. Recipient's Catalog No.
4. Title and Subtitle CAVITATION IN LIQUID CRYOGENS IV - COMBINED CORRELATIONS FOR VENTURI, HYDROFOIL, OGIVES, AND PUMPS		5. Report Date OCTOBER 1974
		6. Performing Organization Code
7. Author(s) J. Hord		8. Performing Organization Report No. None
		10. Work Unit No.
9. Performing Organization Name and Address National Bureau of Standards 325 Broadway Boulder, Colorado 80302		11. Contract or Grant No. C-39004B
		13. Type of Report and Period Covered Contractor Report
12. Sponsoring Agency Name and Address National Aeronautics and Space Administration Washington, D.C. 20546		14. Sponsoring Agency Code

15. Supplementary Notes

Final Report. Project Manager, Werner R. Britsch, Fluid System Components Division, NASA Lewis Research Center, Cleveland, Ohio

16. Abstract

This is the fourth and final volume on the results of a series of experimental and analytical cavitation studies. Previous volumes contain basic analyses and experimental data for a venturi, a hydrofoil, and three scaled ogives. Cross-correlation of the developed cavity data for these five hydrodynamic bodies is performed in this report. The data, for liquid hydrogen and liquid nitrogen, are correlated by using the extended theory derived in Volume II (CR-2156). The new correlating parameter, MTWO, improves data correlation for these sationary bodies and for pumping equipment. The results of this study are applied to the cavitating pump impeller and inducer data published by the NASA Lewis Research Center. Existing techniques for predicting the cavitating performance of pumping machinery are extended to include variations in flow coefficient, cavitation parameter, and equipment geometry. The new predictive formulations hold promise as a design tool and universal method for correlating pumping machinery performance. Application of these predictive formulas requires prescribed cavitation test data or an independent method of estimating the cavitation parameter for each pump. The latter would permit prediction of performance without testing; potential methods for evaluating the cavitation parameter prior to testing are suggested. Directions for future work are indicated.

17. Key Words (Suggested by Author(s)) Cavitation; Cryogenics; Hydrofoil; Impellers; Inducers; Ogives; Pumps; Venturi	18. Distribution Statement Unclassified - unlimited Category 12

19. Security Classif. (of this report) Unclassified	20. Security Classif. (of this page) Unclassified	21. No. of Pages 103	22. Price* $4.50

CONTENTS

CONTENTS (Continued)

LIST OF FIGURES

LIST OF TABLES

CAVITATION IN LIQUID CRYOGENS
IV - COMBINED CORRELATIONS FOR
VENTURI, HYDROFOIL, OGIVES, AND PUMPS

J. Hord

1. SUMMARY

This document is the fourth and final volume to be issued on the results of cavitation studies performed at the NBS. The first, second, and third volumes dealt with venturi, hydrofoil, and ogive experiments and extended the theory for correlating developed cavitation data. This final volume extends these experimental data and correlative expressions to the prediction of cavitating pump performance.

It was emphasized in the previous reports that cryogenic liquids require less subcooling to avoid cavitation; i. e. , less Net Positive Suction Head (NPSH) is required for the cryogens--liquid hydrogen and liquid nitrogen were used in the NBS tests.

Developed cavity data, consisting of pressure and temperature measurements within fully developed hydrogen and nitrogen cavities, were acquired for a venturi, hydrofoil, and three scaled, quarter-caliber ogives. These combined data are correlated herein using the extended theory derived in Volume II of this report series. Maximum benefit, in correlation of these combined stationary-body data, is obtained by using the new MTWO parameter. MTWO is a liquid phase velocity ratio derived from two-phase flow considerations. It is significant that the parameters which satisfactorily correlated the individual venturi, hydrofoil, and ogive data also adequately correlated these combined data. Consequently, these correlating parameters are proven applicable to a variety of body geometries (two-dimensional and axisymmetric) that encompass internal and external cavitating flows.

The new and old correlating expressions are extended herein to apply to rotating machinery. The old expressions were modified to account for size effects in pumps. The size-effect data obtained with the scaled ogives were used. Previous pump prediction work has been restricted to those conditions where pump geometry, flow coefficient and $\Delta H_c / \Delta H_{nc}$ are held constant while fluid, fluid temperature and rotative speed are permitted to vary. This study indicates that existing correlating expressions may be used with much greater latitude-- only $\Delta H_c / \Delta H_{nc}$ must be held constant. This is a significant extension of the state-of-the-art and requires development of an independent method for estimating $K_{c,min}$ of pumping equipment.

Suggestions for estimating $K_{c,min}$ are advanced herein. All currently envisioned methods require detailed knowledge of the pump geometry. Compilation of data relating the experimental cavitating pressure coefficient, $K_{c,min}$, to the calculated noncavitating pressure coefficient, C_p^v, are needed to evaluate these suggestions.

Briefly, this study produced a simplified and precise technique for computing B-factors. The B-factor concept appears to be the most successful approach to predicting cavitation performance of pumps. Analysis of convective heat transfer and mass flux limiting processes resulted in improved correlative— predictive expressions applicable to pump design and operation. Extensive developed-cavity data were acquired for stationary hydrodynamic bodies immersed in a flowing cryogenic liquid. These data were satisfactorily correlated using the improved semi-empirical correlative expressions. These expressions were extended to predict cavitating pump performance. NASA-LeRC liquid hydrogen pump data were used to demonstrate the adequacy of this extension. It was shown that the ability to predict cavitating performance of pumps can be significantly extended. The extension

of semi-empirical correlating expressions from stationary-bodies to pumping machinery was substantiated. Directions for future technical effort were discussed.

2. INTRODUCTION

Cavitation is usually categorized as gaseous or vaporous; in this study we are concerned only with vaporous cavitation. Over the past 30 years much confusion in the cavitation literature is attributable to the failure of authors to clearly recognize and/or categorize their cavitation data. The presence of dissolved gases, minerals, and particulate matter adversely affects the cavitating performance of equipment and simultaneously complicates analysis and data correlation. All data treated in this report are considered to be virtually free of these effects--such are the advantages of cryogenic test fluids. Vaporous cavitation is the formation of a vapor phase within the bulkstream of a flowing liquid, or at the interface between a flowing liquid and a solid surface, caused by a reduction in pressure.

To design liquid handling equipment such as pumps and flow-meters, the designer must determine whether cavitation will occur and, in many cases, to what extent. Since the formation and collapse of vapor cavities alter flow patterns, cavitation may reduce the efficiency of pumping machinery [1], [1] produce vibrations, cause flow instabilities, and reduce the precision of flow measuring devices. Collapse of these vapor cavities can also cause serious erosion damage [2] to pump blades, flowmeter vanes, etc. We usually attempt to avoid cavitation but it is sometimes beneficial; therefore, it is desirable to learn how to predict the cavitating performance of equipment. The weight of rocket vehicles can be reduced by designing

---

[1] Numbers in brackets indicate references at the end of this report.

cavitating pumps to operate at higher rotative speeds and lower pro-pellant tank pressures; i.e., the pump is designed to swallow limited quantities of vapor with little degradation of performance. The potential decrease in pump size and weight, offered by higher rotative speeds, has numerous industrial and aerospace applications.

Pumps designed to perform satisfactorily with controlled cavitation normally require an inducer upstream of the main pump rotor. The function of the inducer is to increase the fluid pressure enough to preclude cavitation in the following stage. Inducers may be an integral part of the pump rotor or may be separately mounted on the pump shaft. Inducers permit satisfactory operation of the succeeding pump machinery while appreciable cavitation is occurring on the suction surfaces of the inducer blades. Thus, net positive suction head (NPSH) require-ments for the pump assembly are lowered considerably with little sacrifice in pump performance.

It is difficult to predict the NPSH required for the satisfactory performance of cavitating equipment. NPSH requirements are deter-mined by the complex and combined effects of fluid properties, pump geometry, pump operating point, and heat and mass transfer. This topic is treated in detail herein. The noncavitating performance of hydraulic equipment may be predicted from established similarity laws but cavitating performance is much more difficult to predict from fluid-to-fluid. Recent advances in this area have been made by NASA-LeRC personnel [3-6] and others [7-9], but additional work is required to improve the current technique for predicting cavitating performance of equipment from fluid-to-fluid. The effects of fluid properties on the cavitation performance of equipment are well recognized [10-19] and have been treated in considerable detail in previous reports [20-23].

A more general predictive technique that includes the effects of equipment geometry and size in addition to fluid properties is sorely needed. This report outlines initial efforts in this direction and clearly shows that more knowledge is needed to extend our predictive capability to equipment design. Predicting cavitating performance for a specific fluid-pump combination using test data from a different fluid-pump combination is our ultimate goal.

NASA has undertaken a program [1] to determine the cavitation characteristics of various hydrodynamic bodies and the thermodynamic behavior of different fluids in an effort to obtain improved design criteria to aid in the prediction of cavitating pump performance. The study described herein was conducted in support of this program.

Liquid hydrogen and liquid nitrogen were chosen as test fluids for this study for the following reasons: (1) the ultimate goal of this program is to acquire sufficient knowledge to permit intelligent design of pumps for near-boiling liquids, and (2) predictive analyses indicated [1] that the physical properties of hydrogen and nitrogen make them particularly desirable test fluids. The objectives of this study were (1) to determine experimentally the flow and thermodynamic conditions required to induce desinent (or incipient) and developed cavitation on various hydrodynamic bodies, (2) to improve existing correlative expressions for the prediction of cavitating performance of hydraulic equipment, and (3) to establish, if possible, a technique for predicting the fluid-handling capability of different cavitating equipment using different fluids. The first two objectives have been effectively accomplished and the third item, though ambitious, has been significantly

advanced. The second and third objectives are extensions of the state-of-the-art and more experimental pump data are needed to fully evaluate progress on the last objective.

Due to the bulk of the subject matter, reader familiarity with the first three volumes of this report series is necessary and is assumed throughout this final volume. Definitions, terminology, etc., are consistent throughout this report series. Although desinent and developed cavity data were acquired in the stationary-body tests, only the developed cavity data are of interest in this final volume.

This report summarizes the work performed on five hydrodynamic bodies with three different geometries (shapes). It also documents the analytical and correlative work performed at NBS on the experimental pump data [4, 6] generated by NASA-LeRC personnel. Previous correlative efforts [3-6] and those reported herein indicate that results obtained from stationary-body studies are directly applicable to the correlation and prediction of cavitating pump performance. Cavitation data for the hydrodynamic bodies (venturi, hydrofoil, and ogives), apparatus details, test procedures, etc., were reported in Volumes I, II, and III of this report series [20-22]. These three volumes also contained data correlation efforts for each individual body shape.

A similarity equation, based upon the B-factor concept of Stahl and Stepanoff [11], has been developed [19] for correlating cavitation data for a particular test item from fluid-to-fluid; this correlation is also useful in extending the velocity and temperature range of data for any given fluid. Thermal boundary layer considerations and two-phase

mass flux limiting concepts were used [21] to improve this correlative expression. A new correlating parameter, MTWO, was developed [21] and has proven to be a valuable correlating parameter for our venturi, hydrofoil [21], and ogive [22] data. The MTWO parameter is the ratio of V_o/V_ℓ where V_ℓ is proportional to the two-phase liquid-vapor sonic velocity across the cavity interface, see reference [21]. The correlative expressions [21] developed in the course of this study are used to correlate the combined experimental data for the ogives, hydrofoil, and venturi. In turn, these results are used to develop correlative/predictive equations for pumps and are applied to the NASA-LeRC pump data. These generalized equations account for changes in pump size, geometry, flow coefficient and rotative speed, and for changes in fluid and fluid temperature. Prediction of the cavitating performance of pumping equipment was previously restricted [4-6] to changes in pump rotative speed, fluid, and fluid temperature. More experimental pump data are needed to fully evaluate the new generalized correlative/predictive equations.

An improved method of predicting the cavitating performance of pumping equipment is presented herein. This improved method is an extension of previous correlative efforts [3-6].

3. EXPERIMENTAL EQUIPMENT, INSTRUMENTATION, AND TEST PROCEDURES

The experimental facility, instrumentation, error statements, visual and photographic aids, and test procedures used in this study were fully described in the first volume [20] of this report series. One additional error statement, concerning uncertainty in pressure measurement for nitrogen test fluid, was needed and given in section 5.2 of

Volume II [21]. Geometric and construction details for each body-tunnel configuration were given in the respective reports for the venturi [20], hydrofoil [21], and ogives [22]. Each body-tunnel combination was located between the supply and receiver dewars of a blowdown flow system as previously described [20].

Briefly, the objective of this experimental program was to obtain and analyze desinent and developed cavitation data for various hydrodynamic bodies immersed in flowing cryogenic fluids. This experimental data, combined with an analytical study, was intended to advance existing knowledge of the cavitating performance of equipment. Information concerning model size, geometry, fluid, fluid velocity, and temperature is prerequisite to the improvement or development of a general expression for predicting the cavitation performance of hydraulic equipment. Experimental apparatus consisted of supply and receiver dewars equipped to control fluid state and fluid flow conditions. Instrumented test sections (tunnels) and streamlined bodies were situated between the dewars. Desinent and developed cavitation data were acquired at various fluid temperatures and velocities in liquid nitrogen and liquid hydrogen. Closed circuit television and movie film were used to define and analyze the data--particularly the cavity shape data. High speed data recording was provided by a magnetic tape data-acquisition system. A short description of each hydrodynamic body is given in the following paragraph.

A transparent plastic venturi [20] with a quarter-round stepped throat provided needed data relative to internal flow geometries. Representative data for two-dimensional bodies were acquired for a submerged hydrofoil [21] with cylindrical (half-caliber) leading edge.

The three scaled, quarter-caliber, ogives [22] used in this experiment consisted of submerged cylindrical bodies with quarter-caliber rounded noses. The diameters of these cylindrical bodies varied by a factor of two. These ogive data supplied necessary information relative to size effects and external flow over axisymmetric bodies. The hydrofoil and ogives were sting-mounted and housed in appropriate transparent plastic tunnels; therefore, tests with these bodies permitted us to photographically determine cavity shape as a function of body shape and flow conditions. The hydrofoil and ogive test assemblies were installed in the same space allocated for the plastic venturi [20] in the experimental apparatus.

4. DATA ANALYSIS

We seek to apply the results of this experimental and analytical investigation to the design and operation of liquid pumps. The NASA-LeRC pump impeller and inducer data [4, 6] were chosen to evaluate our predictive expressions. Our data and the NASA-LeRC experimental pump data are correlated and discussed separately in this section.

4.1 Selection of Stationary-Body Data

The data selected were generated during the course of this experimental program. All of the venturi [20], hydrofoil [21] and ogive [22] data were used. Fluid properties for nitrogen [24] and hydrogen [25] are well known and documented. These property data are considered

more accurate than those for water [26] and common refrigerants [27]
Other applicable published stationary-body data [3, 19, 28] were not used
because (1) they were not available in sufficient detail or quantity, or
else (2) they were acquired using test fluids having poorly defined fluid
properties. The need for accurate fluid property data cannot be over-
emphasized, as small uncertainties in property data can result in large
uncertainties in calculated B-factor [23]--a vital constituent of our
correlative-predictive expressions.

4.2 Correlation of the NBS Stationary-Body Data

Previous reports [20-22] have documented correlative efforts for
each body shape. In this final volume the combined venturi-hydrofoil-
ogive (VHO) data are correlated. Knowledge of fluid properties, flow
conditions, body geometry, and cavity lengths are required. The
visual cavity lengths, as determined from movie film, were used in all
correlative data fits.

Pressure and temperature profiles within fully developed cavities
were measured and are referred to herein as developed cavitation data.
The bulkstream vapor pressure exceeds the measured cavity pressure;
it also exceeds the saturation pressure corresponding to the measured
cavity temperature. Therefore, the measured pressure depressions
and the pressure depressions corresponding to the measured temperature
depressions are called "pressure depressions." Alternatively, the
pressure depression may be expressed in terms of its equivalent equili-
brium "temperature depression." The state of thermodynamic equilibrium
within the developed cavities was determined from these direct measure-
ments of pressures and temperatures within the vaporous cavities. Cavitie:
developed on the hydrofoil [21] and ogives [22] were in stable thermo-
dynamic equilibrium. Metastable vapor was found to exist in the central

10

and aft regions of hydrogen cavities developed inside of the venturi [20].
Stable thermodynamic equilibrium prevailed near the leading edge of
the cavities for all of the VHO data. Earlier analytical work [20, 21]
indicated that this thermodynamic condition was sufficient for compati-
bility of theory and experiment.

The VHO developed cavity data are correlated [20] by using the
experimental values of cavity pressure and temperature depressions.
The pressure depression in the cavitated region is determined by
subtracting the measured cavity pressure, in one case, and the satura-
tion pressure associated with the measured cavity temperature, in the
other case, from the vapor pressure of the liquid entering the test
section. Profiles of measured pressure depression for all of the VHO
data were presented and thoroughly discussed in previous reports
[20 - 22]. Pressure depression is maximum at the leading edge of the
cavity and zero at the trailing edge of the cavity. Maximum pressure
depressions for the VHO data are tabulated below.

Table 4. 1   Maximum pressure depressions for the VHO
developed cavity data.

Hydrodynamic Body	Test Fluid	Maximum Pressure Depression
Venturi [20]	hydrogen	15. 13 psi (10. 44 N/cm^2)
Hydrofoil [21]	hydrogen	15. 76 psi (10. 87 N/cm^2)
Hydrofoil [21]	nitrogen	10. 08 psi (6. 96 N/cm^2)
Ogive [22]	hydrogen	13. 77 psi (9. 50 N/cm^2)
Ogive [22]	nitrogen	12. 89 psi (8. 89 N/cm^2)

The correlative expressions, developed in a previous report [21], were used to correlate the developed cavity data from the VHO experiments. The two correlative equations are given as follows:

$$\frac{B}{B_{ref}} = \left(\frac{\alpha_{ref}}{\alpha}\right)^{E1} \left(\frac{V_o}{V_{o,ref}}\right)^{E2} \left(\frac{\ell}{\ell_{ref}}\right)^{E3} \left(\frac{\nu_{ref}}{\nu}\right)^{E4} \left(\frac{\sigma_{ref}}{\sigma}\right)^{E5} \left(\frac{D}{D_{ref}}\right)^{E6}$$

(4-1)

$$\frac{B}{B_{ref}} = \left(\frac{\alpha_{ref}}{\alpha}\right)^{E1} \left(\frac{MTWO}{MTWO_{ref}}\right)^{E2} \left(\frac{\ell}{\ell_{ref}}\right)^{E3} \left(\frac{\nu_{ref}}{\nu}\right)^{E4} \left(\frac{\sigma_{ref}}{\sigma}\right)^{E5} \left(\frac{D}{D_{ref}}\right)^{E6}$$

(4-2)

Equation (4-1) is an improved and extended version [21] of the simplified correlative expression developed by Gelder, et al. [19]. Equation (4-2) was derived [21] from basic heat and mass transfer considerations in Volume II of this report series. These expressions, along with the isentropic BFLASH theory [23] and two least-squares data-fitting computer programs [20], were used to correlate the combined VHO data. These equations are used to correlate developed cavitation data in similar test items and to predict the cavitation performance of a test item from fluid-to-fluid, or at another temperature of the same fluid, when limited test data from a single fluid are available. They are also used herein to correlate developed cavity data from one hydrodynamic body to another and to predict cavitation performance from one pump to another. First, we concentrate on the stationary-body data.

Complete and detailed descriptions of the correlative technique, computational steps, and computer programs are given in reference [20]. The correlative procedure, as previously described [20], can be

followed directly when using eq (4-1). To use eq (4-2), simply sub-
stitute MTWO for V_O in the computer program. Briefly, this correlative
procedure ensures that the B values calculated from eq (4-1), or eq (4-2),
and the BFLASH values [23] for each data point are as nearly identical
as possible; both B values at each data point are evaluated from experi-
mental data and this correlative procedure produces the best possible
agreement between the isentropic flashing theory [23] and the correla-
tive expression--eq (4-1) or eq (4-2). This "best-fit" of the experi-
mental data is obtained by selecting appropriate exponents for each of
the correlative parameters in the correlative expression--eq (4-1) or
eq (4-2). The exponent selecting process is quite complex and is treated
in appropriate detail in reference [20]. Exponents for eq (4-1) and
eq (4-2) were derived to evaluate the suitability of MTWO as a correlat-
ing parameter for the combined venturi, hydrofoil, and ogive data. One
should recall that the individual venturi, hydrofoil, and ogive data
correlations were significantly improved [22] by use of the MTWO
parameter; similar improvement was obtained with the combined VHO
data.

In eq (4-1) and eq (4-2) the cavity lengths were evaluated at the
visually observed lengths. BFLASH was obtained for each experi-
mental data point by using T_O, the maximum measured cavity pressure
depression, and the calculation method outlined in reference [23]. The
fluid physical properties are evaluated at P_O and T_O with the exception
that MTWO is evaluated at the minimum measured cavity pressure.
The characteristic dimension, D, was taken as the contour radius for
each hydrodynamic body because all three body shapes possess a constant
radius contour upon which the cavity originates. The standard deviation in
B is computed for each set of exponents; the individual exponents may be

held constant or be chosen by the computer. The standard deviation in B factor is minimized in the computer programs when one or more of the exponents is selected by the computer; the absolute minimum standard deviation is obtained when all of the exponents are selected by the computer as in this report. In those cases where the exponents are held constant, the standard deviation cannot be minimized and is merely computed. The set of exponents that produces minimum standard deviation in B is selected as the best solution for any particular batch of data; i.e., the standard deviation is a measure of the validity of the correlative theory and of the isentropic-flashing theory, as both are evaluated from experimental data.

Because MTWO proved to be a valuable correlating parameter for the individual venturi, hydrofoil, and ogive data [22], the combined VHO data were correlated with and without the MTWO parameter to further evaluate its influence. Correlation of the combined VHO data with eq (4-1), and then with eq (4-2), provides direct evaluation of MTWO as a correlating parameter--identical comparisons were prepared for the individual venturi, hydrofoil, and ogive data [22]. Table 4.2 summarizes the individual and combined correlative results for developed cavitation on all geometries (bodies) tested in this study, i.e., venturi, hydrofoil, and ogives. The results given in table 4.2 are discussed in the following section of this report.

4.3 Discussion of the NBS Stationary-Body Data

Cavity visual appearance, interpretation of data, and graphical display of typical developed cavity data were treated in detail in previous reports [20-22]. In this final volume we concentrate on our efforts to correlate the combined data for the VHO. In brief, the pressure

Table 4.2 Summary of correlative results for developed cavity data--venturi, hydrofoil, ogives, and combined venturi-hydrofoil-ogives (VHO).

Line No.	Hydrodynamic Body	Test Fluids	Correlative Equation	Source of Data	Exponents					Ref. Run No.	Standard Deviation in B-Factor [†]	Mean Percent Difference in B-Factor [††]	$\overline{K}_{c,min}$
					E1	E2	E3	E4	E6				
1	Venturi	H_2	(4-2)**	This Study [20]	(0.10)	0.59	0.18	---	---	071C	0.2234	5.5	2.459
2	Hydrofoil	H_2 & N_2	(4-2)	This Study [21]	(-0.13)	0.59	0.27	---	---	255B	0.2565	9.9	1.833
3	Ogives	H_2 & N_2	(4-2)	This Study [22]	(-0.05)	0.43	0.25	---	0.59	338B	0.2126	11.1	0.531
4	VHO	H_2 & N_2	(4-2)	This Study	---	0.51	0.28	---	0.43	338B	0.2618	11.7	---
5	Venturi	H_2	(4-1)*	This Study [20]	-1.92	0.74	0.31	---	---	071C	0.3466	9.0	2.459
6	Hydrofoil	H_2 & N_2	(4-1)	This Study [21]	0.80	0.64	0.45	-1.00	---	255B	0.3717	12.7	1.833
7	Ogives	H_2 & N_2	(4-1)	This Study [22]	0.32	0.21	0.34	-0.84	0.60	338B	0.2620	14.3	0.531
8	VHO	H_2 & N_2	(4-1)	This Study	---	0.11	0.36	---	0.58	338B	0.4311	16.3	---
9	Venturi	H_2 & F-114	(4-1)	Reference [3]	1.0	0.8	0.3	---	-0.10	---	---	---	2.47

$*$ $\dfrac{B}{B_{ref}} = \left(\dfrac{\alpha_{ref}}{\alpha}\right)^{E1} \left(\dfrac{V_o}{V_{o,ref}}\right)^{E2} \left(\dfrac{\ell}{\ell_{ref}}\right)^{E3} \left(\dfrac{\nu_{ref}}{\nu}\right)^{E4} \left(\dfrac{\sigma_{ref}}{\sigma}\right)^{E5} \left(\dfrac{D}{D_{ref}}\right)^{E6}$ ---eq (4-1).

$**$ $\dfrac{B}{B_{ref}} = \left(\dfrac{\alpha_{ref}}{\alpha}\right)^{E1} \left(\dfrac{MTWO}{MTWO_{ref}}\right)^{E2} \left(\dfrac{\ell}{\ell_{ref}}\right)^{E3} \left(\dfrac{\nu_{ref}}{\nu}\right)^{E4} \left(\dfrac{\sigma_{ref}}{\sigma}\right)^{E5} \left(\dfrac{D}{D_{ref}}\right)^{E6}$ ---eq (4-2).

$\dagger$ Standard Deviation $\equiv \sqrt{\left[\sum (B-B_t)^2\right]/(NPTS-1)}$, where NPTS = number of data points (including "ref" data point), B_t = BFLASH and is computed from isentropic-flashing theory [23], and B is computed from eq (4-1) or eq (4-2).

$\dagger\dagger$ Mean Percent Difference $\equiv \left[\sum\left\{|B-B_t|(100/B_t)\right\}\right]/(NPTS-1)$.

depressions obtained from the cavity temperature measurements were generally in good agreement with those derived from the measured pressures for the ogives and hydrofoil, i.e., within the allowances of instrument error the cavity vapor was in stable thermodynamic equilibrium. Evidence of metastable vapor was presented in the venturi study [20]. The VHO data revealed that cavity pressure depressions generally increase with increasing cavity length, body size, fluid temperature, and velocity; however, the pressure depressions decrease with increasing velocity for the two smallest ogives tested in liquid hydrogen. Similar results were obtained in pump inducer performance tests [6] using liquid hydrogen.

These cavity parameter functional dependencies are also shown by tabulating the values of the exponents derived to fit the experimental data--see table 4.2. In reference [23] it is shown that the pressure depression increases with increasing T_o and B. Referring to line 4 of table 4.2 we observe that B increases with increasing V_o, ℓ, and D for the VHO data. Then, for these data, the pressure depression must increase with increasing T_o, V_o, ℓ, and D. By inspecting the exponent data in table 4.2, similar deductions may be drawn for the various body-fluid combinations tested.

4.3.1 Mathematical Correlative Results

Equations (4-1) and (4-2) were fitted with numerical exponents derived by forcing these equations to fit the venturi, hydrofoil, and ogive experimental data. These equations were derived in the course of this study [22] and represent extensions of the work of Gelder, et al. [19]. The exponents given in table 4.2 were obtained with a least-squares fitting technique and a digital computer; the suitability of the various exponents to the experimental data is indicated by the standard

16

deviation in B-factor as explained previously. The mean percent difference in B-factor, as defined in table 4.2, may also be used to assess the perfection of the correlative data fit. In the hydrogen venturi data the value of B ranges from 2.0 to 5.0; in the hydrofoil experiments the value of B ranges from 1.0 to 5.0 for both hydrogen and nitrogen; in the ogive data the value of B ranges from 0.7 to 2.8 for hydrogen and from 0.5 to 3.0 for nitrogen.

The expressions used to correlate the experimental data are given at the bottom of table 4.2. The mathematical technique used to derive the exponents can easily pick an extraneous value for any of the exponents if there does not exist significant variation in the corresponding physical parameter. This point has been elaborated upon in previous reports [20-22] and will not be discussed here; however, it is the lack of variation in α that explains why E1 tends toward a negative number in line 5 of table 4.2. In lines 1, 2, and 3 of table 4.2 the numerical value of E1 is so small that the α term could be ignored. The variation in α for the hydrogen-nitrogen correlations was about 2:1. There was more than 400 percent change in α in the hydrogen-refrigerant 114 data correlated by Moore and Ruggeri [3], and therefore the value for E1 reported in line 9 of table 4.2 is preferred when correlating with eq (4-1). It is apparent that the combined fluid correlations, for any hydrodynamic model or correlative expression, are to be preferred because of the greater variation in physical parameters.

In all of our individual venturi, hydrofoil, and ogive data, use of the ν and σ terms improved the correlations; however, it is felt that use of these additional correlating parameters is not justified unless they substantially improve the correlative fit. None of the data were materially improved by the use of σ; therefore, values for E5 are not

included in table 4.2. Similarly, the ν term was of value only for some of the combined fluid correlations using eq (4-1) (see values for E4 in table 4.2). Because the σ term was of negligible value in the correlative fit, even though it varied by a factor of three, we must conclude that σ is not an important correlating parameter for the cryogens tested; however, it may yet prove to be a valuable correlating parameter for other fluid combinations. Also, ν may be an excellent correlating parameter for other fluid combinations and is of considerable value for some of the hydrogen-nitrogen combinations. Correlation of the hydrogen-refrigerant 114 data (line 9 of table 4.2) would most likely be improved by using one or both of these terms.

Inspection of the first four lines of table 4.2 shows that E1 is negligible and E2, E3, and E6 are relatively consistent for the data correlated using eq (4-2). No such consistency exists when correlating the data with eq (4-1) (see lines 5 through 9 in table 4.2). That eq (4-2) is quite superior to eq (4-1), as a correlative expression, is readily shown by line-to-line comparison of the results given in table 4.2. A substantial reduction in standard deviation in B-factor (or mean percent difference in B-factor) is achieved in all cases where eq (4-2) is used-- compare lines 1 and 5, 2 and 6, 3 and 7, 4 and 8. The use of MTWO is clearly superior to the use of V_o as a correlating parameter. Careful study of the data in table 4.2 shows that the numerical values of E1, E3, ⎺6 are reduced when eq (4-2) is used. The effect of the α term is d ecause of the many thermophysical and thermodynamic fluid pro embodied in the MTWO parameter. The predominant influence of tl /O term must also be responsible for the reductions in E3 and L .nen eq (4-2) is used. The importance of MTWO as a correlating parameter emphasizes that mass transfer plays an important role in the cavitation process.

18

Perusal of the E6 data in lines 3 and 4 reveals that the size effect is more pronounced for the scaled ogives than for the combined VHO data. Superficially, it appears that the value of E6 in line 4 should be favored because it correlates data for three different body shapes; however, each body shape has constant-radius contours. Consequently, it is not yet clear whether the VHO exponents (line 4) or the scaled ogive exponents (line 3) should be selected for future use. Both sets of exponents were used herein to correlate pump data and produced nearly identical results. The nearly negligible value of E6 given in line 9 of table 4.2 may be attributable to the small scale ratio (1.414:1) used in the refrigerant-114 tests [3]. Billet [28] used water and refrigerant-113 to test 0.24-inch and 0.50-inch diameter zero-caliber ogives. He obtained values of E1 = 0.60, E2 = 0.30, E3 = 0.58, and E6 = -0.25 for these tests--as derived from a formulation similar to eq (4-1). Thus, it appears that size effects can vary with equipment geometry. The experimental data represented in lines 3 and 4 are far more extensive, and the values of E6 are much more consistent from body-to-body than the earlier work [3, 28]; therefore, the size effects indicated by lines 3 and 4 are to be preferred.

Excluding size effects, line 9 represents the maximum variation in correlating parameters when eq (4-1) is used. Thus, E1, E2, and E3 from line 9 were combined with E6 from line 8 (or line 7) to produce an improved expression with the form of eq (4-1) for use in pump correlation work, i.e., E1 = 1.0, E2 = 0.8, E3 = 0.3 and E6 = 0.6 in eq (4-1). Alternatively, we could have used the exponent sets from lines 7 or 8 for comparative correlations of pump data. The latter choices were rejected because (1) the exponent sets in lines 7 and 8 are quite inferior to those of lines 3 and 4, and (2) the E1, E2, E3

values in line 9 have been moderately successful in previous pump correlations [4-6]. Equipping eq (4-1) with E1, E2, and E3 from line 9 and with E6 from line 8 produces an improved correlative expression of the original simplified form [4]. This expression can then be compared with eq (4-2)--equipped with exponents as in lines 3 or 4 of table 4.2--in predicting cavitating pump performance.

Attempts were made to improve the VHO data correlation (line 4 of table 4.2) using new correlating parameters. Simultaneously considering (1) the rate [20] at which a particle of liquid traverses a sub-saturation pressure region in cavitating equipment, and (2) the theoretical heat and mass transfer processes outlined in Volume II [21], several potential correlating parameters may be contrived. Each new parameter may then be evaluated by substituting them one at a time into eq (4-2) and correlating the VHO data. The new parameter may be inserted in place of the α, ν, or σ terms in eq (4-2). If use of the parameter results in a reduction of standard deviation in B-factor, the parameter could be retained for future use. None of the newly contrived parameters offered sufficient promise to warrant retention.

The parameters tried were δ, δ/D, ℓ/δ, K_v, $K_{c,min}$, $\overset{v}{C}_p$, $\overset{v}{C}_p/K_{c,min}$, $\overset{v}{C}_p/\delta$, $\delta\overset{v}{C}_p$, $\overset{v}{C}_p V_o^2/2g_c\delta$, $h_o - \overset{v}{h}$, $(h_o - \overset{v}{h})/\delta$, $\dfrac{(h_o - \overset{v}{h})}{\delta}\left[1 + (1 - \overset{v}{C}_p)^{1/2}\right]$, $h_v - \overset{v}{h}$, NPSH, $(NPSH + h_v - \overset{v}{h})$, A_o, D_o, F_C, and F_B (all symbols are identified in the nomenclature section of this report). Because the three body shapes evaluated have constant-radius contours the $\delta/D \approx$ constant for all three geometries; therefore, substitution of δ for D in eq (4-2) produces almost identical results. It is felt that δ could be an important parameter in correlating other stationary-body data and in correlating pump data. In accordance with

the arguments presented in the dimensional analysis of Volume II [21],
several Dimensionless Numbers were also tried as correlating parame-
ters. None of them improved the correlative fit for the VHO data--Fr,
We_ℓ, Re_ℓ, Pr, Re_D, and Pe were tried in eq (4-2).

4.3.2 Influence of Body Shape, Fluid, and Size on $K_{c,min}$

Variations in $K_{c,min}$ from body-to-body and fluid-to-fluid were
previously [22] discussed in detail; however, this topic is so pertinent
to the correlation of pump data that it will be summarized here.

The arithmetic mean value of the developed cavitation parameter,
$\overline{K}_{c,min}$, does not vary appreciably for the venturi data presented in
table 4.2. This parameter was also relatively constant for the hydrofoil
data [21]; this is an important result, because constant $\overline{K}_{c,min}$, eq
(4-1), and the isentropic flashing theory [23] are used to predict [4,5]
the cavitating performance of a particular piece of equipment. The
fact that $\overline{K}_{c,min}$ is different for different bodies curtails the current
predictive techniques [4,5] to a particular piece of equipment; i.e., the
geometry (shape) of the cavitating equipment must be identical or simi-
lar. Actually, it was anticipated [20] that $\overline{K}_{c,min}$, for many cavitating
bodies, would not remain constant--as with the venturi--for all fluids,
cavity lengths, velocities, temperatures, etc. Then, it was neither
surprising that $\overline{K}_{c,min}$ for the hydrofoil varied slightly [21] nor that
$\overline{K}_{c,min}$ varied appreciably with the ogive body-fluid combinations [22].
For the ogive data, $\overline{K}_{c,min}$ varied by a factor of 1.5:1.

Also, $K_{c,min}$ varied more for the ogives and the hydrofoil than
for the venturi; $K_{c,min}$ was within 7 percent of $\overline{K}_{c,min}$ for the venturi
and within 15 percent for the hydrofoil. $K_{c,min}$ for the ogives varied
as follows: 1) 0.210-inch ogive--$K_{c,min}$ varied from 0.33 to 0.51
with hydrogen and from 0.36 to 0.63 with nitrogen, 2) 0.357-inch

ogive--$K_{c,min}$ varied from 0.50 to 0.77 with hydrogen and from 0.43 to 0.71 with nitrogen, 3) 0.420-inch ogive--$K_{c,min}$ varied from 0.53 to 0.71 with hydrogen and from 0.45 to 0.63 with nitrogen. From these data, it is apparent that $K_{c,min}$ increases with increasing ogive size. The 0.24-inch diameter zero-caliber ogive data of Billet [28] for water and refrigerant-113 show similar variations in $K_{c,min}$ (0.32 to 0.52). Also, significant variations in $K_{c,min}$ have been detected in pump impeller [4] and pump inducer [5,6] performance tests. Then, for a specific piece of equipment $K_{c,min}$ can vary appreciably with fluid and flow conditions, and $K_{c,min}$ for similar equipment can be expected to vary with size.

An unsuccessful attempt was made to establish a functional dependency of $K_{c,min}$ upon ℓ, V_o, and T_o for these stationary-body data. For the venturi [20], $K_{c,min}$ is nearly independent of ℓ, V_o, and T_o. The hydrofoil $K_{c,min}$ is nearly independent of ℓ and V_o and increases very slightly with increasing T_o. Likewise, with the ogives, $K_{c,min}$ is almost independent of ℓ and V_o and increases with increasing T_o. Billet obtained different results for zero-caliber ogives [28]--$K_{c,min}$ decreased with increasing ℓ, increased slightly with increasing V_o, and was nearly independent of T_o. Consequently, the behavior of $K_{c,min}$ for different equipment is not currently predictable prior to testing.

Where $K_{c,min}$ does not vary appreciably, it is convenient to use $\overline{K}_{c,min}$ for predictive purposes. With large variations in $K_{c,min}$, as in our ogive data, this practice will produce relatively crude predictive results; however, in practical applications similar flow conditions can sometimes be selected [4-6] so that predictions can be made at identical values of $K_{c,min}$. Data presented herein shows that $K_{c,min}$, and consequently $\overline{K}_{c,min}$, varies widely with body or equipment

geometry, as does the pressure coefficient, C_p. Thus, it is quite obvious that prediction of cavitation performance, from one piece of equipment to another, will require significant advances in the determination of $K_{c,min}$ as functions of body geometry, fluid, body size, ℓ, V_o, and T_o.

As a preliminary step, we can supply, from this study and others, data that relates $\overline{K}_{c,min}^v$ to the noncavitating minimum pressure coefficient, C_p^v. The definitions of these two parameters are nearly identical, except that $\overline{K}_{c,min}^v$ is based upon minimum cavity pressure in cavitating flow and C_p^v is based upon minimum pressure in noncavitating flow--also, C_p^v has a negative numerical value (see nomenclature). Experimental data from this study and others are plotted on figure 4.1; $K_{c,min}$, $\overline{K}_{c,min}^v$, and C_p^v are not corrected for blockage in the upper curves on this plot. In the lower curve $\overline{K}_{c,min}$ has been corrected for blockage and is plotted as $(\overline{K}_{c,min}^v)_\infty$. If a designer can estimate values of C_p^v from idealized fluid flow solutions or from model scale-up tests in wind tunnels, a corresponding value of $\overline{K}_{c,min}$ can be picked from figure 4.1. It may then be possible to apply the predictive techniques outlined in the later sections of this report to estimate cavitation performance from one piece of equipment to another.

4.3.3 Developed Cavity Shapes

One of the main objectives of the hydrofoil and ogive experiments was to obtain cavity volume-thickness data in an effort to improve the correlative theory. The hydrofoil and ogive cavity shape data were fully discussed in previous reports [21, 22] and are briefly summarized here. Cavity thickness and volume increased with increasing cavity length and were nearly independent of V_o and T_o. The shapes of all of the cavities were adequately represented over the front halves of the cavities by a simple algebraic expression of the form $\delta_v = C_o x^p$, where δ_v and x
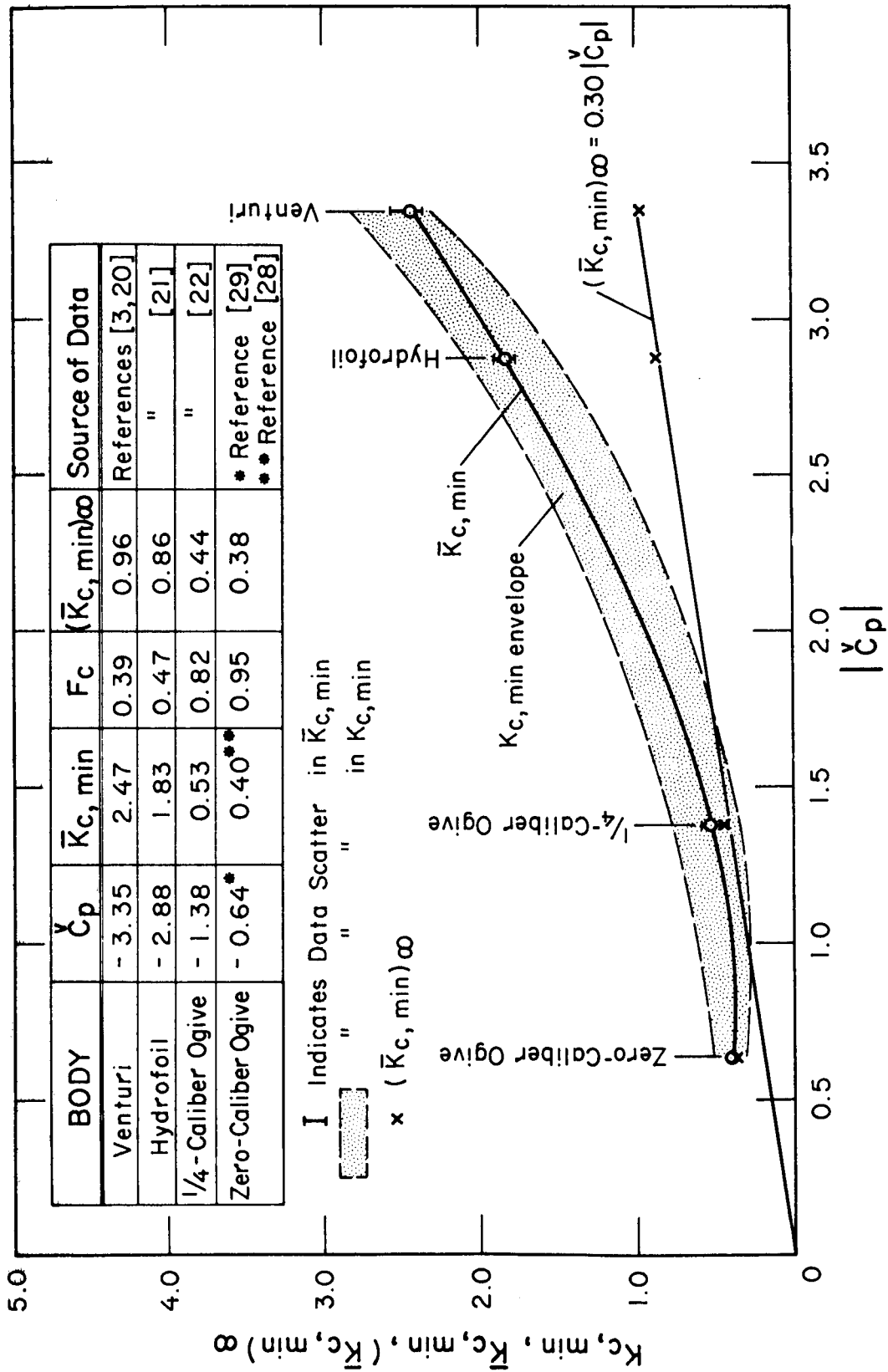
Figure 4.1 Variation of minimum cavitation parameters with minimum non-cavitating pressure coefficient, $\check{C}_p$, for various hydrodynamic bodies.

BODY	$\check{C}_p$	$\bar{K}_{c,min}$	F_c	$(\bar{K}_{c,min})\infty$	Source of Data
Venturi	-3.35	2.47	0.39	0.96	References [3,20]
Hydrofoil	-2.88	1.83	0.47	0.86	" [21]
1/4-Caliber Ogive	-1.38	0.53	0.82	0.44	" [22]
Zero-Caliber Ogive	-0.64*	0.40**	0.95	0.38	* Reference [29] ** Reference [28]

$\mathbf{I}$ Indicates Data Scatter in $\bar{K}_{c,min}$

in $K_{c,min}$

$\times$ $(\bar{K}_{c,min})\infty$

$(\bar{K}_{c,min})\infty = 0.30\,|\check{C}_p|$

are in millimeters and x cannot exceed $\ell/2$. The mathematical expressions [22] for the scaled-ogive cavity shapes were reasonably consistent and are approximated by $\delta_v \approx 0.41 \, x^{0.75}$.

4.4 Selection of Pump Impeller and Inducer Data

The NASA-LeRC [4, 6] impeller and inducer data using liquid hydrogen test fluid were used. Other published data [8, 9, 12, 16, 18] were rejected for failing to meet one or more of the selection criteria cited below.

In order to correlate cavitation performance from pump-to-pump, we need precise information about (1) the geometry of each pump, (2) cavitation performance characteristics for each fluid and each pump, (3) instrumentation uncertainties, (4) pressure depression vs B-factor characteristics for each fluid, and (5) the uncertainties in fluid property data. Some of these selection criteria are interrelated, but each is of sufficient importance to warrant separate discussion.

1) Pump geometry: Geometrical details of pumping equipment are usually not published along with the pump performance data. This may be partially attributed to protection of proprietary design information and partially to the complexity and burden of accurately describing such equipment. The pump inlet area and the impeller and inducer tip diameters are essential information while blade angle, blade tip solidity, blade configuration, etc., are highly desirable parameters for future correlative work. Even the highly detailed geometrical data published by NASA [4, 6, 30-32] were inadequate for some of the analysis performed herein--supplementary data were obtained by personal communication [33]. Thorough documentation of pump geometry, including scaled drawings and photographs, will be necessary in future work. The NASA-LeRC publications [6, 31, 32] contain good examples of the required information.

2) <u>Cavitation performance characteristics</u>: Typical performance data are normally given at restricted or singular values of the flow coefficient ϕ. To correlate cavitating pump performance from one pump to another requires the use of complete pump performance data. NPSH-ΔH curves at constant values of N, T_o, and ϕ simplify the correlative procedure. From these data it is possible to determine ΔH_{nc} and then ΔH_c for a prescribed value of ψ'. Low values of ψ' (approximately 0.7) may be picked to provide the best available NPSH data. Higher values of ψ' require more precise measurement of NPSH and more precise determination of ΔH_{nc} because the slopes of the NPSH - ΔH curves are flatter at higher values of ψ'--typical NPSH-ΔH curves are shown on figure 4.2. Most published data use very high values of ψ' (0.97 or 0.98) which effectively amplify the uncertainties in measured NPSH and ΔH_{nc}. Complete NPSH - ΔH data are available for the NASA-LeRC pump impellers [4,31,32] and inducers [5,6,34-36].

3) <u>Instrumentation uncertainties</u>: The precision of pump performance data is frequently difficult to assess because instrument uncertainties are not clearly stated. Knowledge of the uncertainties in the measurement of NPSH, ΔH, T_o, N, and flow is required to perform accurate correlations or predictions. Performance data with cryogens or conventional liquids, such as water, require very precise measurement of temperatures and pressures. The steep slope of the saturation pressure-temperature curve for water signifies that small errors in temperature measurement can introduce large errors in NPSH. Predictive work with water is further complicated because cold water exhibits low values of Δh_v, and vaporous cavitation effects are sometimes masked by gaseous cavitation. Thus, instrumentation requirements [9] for water correlations are very exacting. It is common knowledge that precise thermometry instruments are needed when cryogenic test fluids are used.

(a) Nominal hydrogen temperature, 31.0° R (17.2 K).

(b) Nominal hydrogen temperature, 34.1° R (18.9 K).

(c) Nominal hydrogen temperature, 36.5° R (20.3 K).
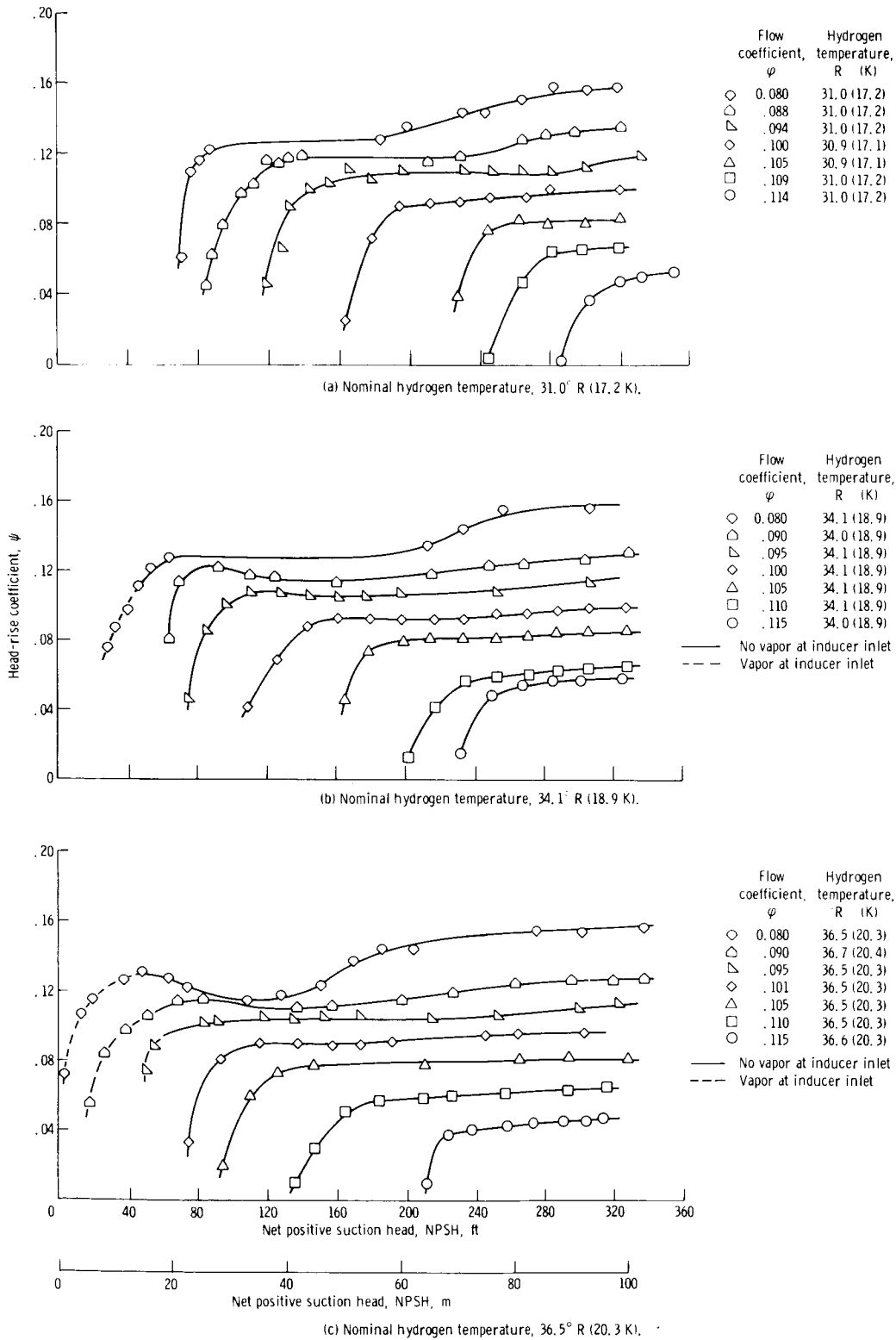
Figure 4.2 Typical cavitation performance data [34] for 80.6° helical inducer pumping liquid hydrogen (N = 30 000 rpm).

27

4) Δh_v vs B-factor: The B-Δh_v characteristics of each fluid are markedly different [23]. Δh_v varies almost linearly with B-factor for water, but Δh_v is a nonlinear function of B for the common cryogens [23]. Cold water and other conventional liquids, with boiling points near room temperature, characteristically exhibit relatively low values of Δh_v. In contrast, cryogenic fluids show relatively large values of Δh_v. Fluid properties must be accurately known to produce accurate B - Δh_v data.

5) Fluid property uncertainties: Fluid property data are simply inadequate for most conventional fluids--particularly hydrocarbons [9, 16, 18][2]; water properties are in many respects still marginally defined even though much effort has been expended in this area [26, 37, 38]. A discontinuity in the saturation temperature-entropy data for refrigerant-113 [27] does not encourage its use as a test fluid. As a result of stringent aerospace and cryogenic industry demands, thermophysical properties of most pure cryogenic fluids [24, 25, 39-43] are better known. Because of particle-physics and aerospace emphasis, the transport and thermodynamic properties of parahydrogen [43, 44] are probably the most extensive and precise. It was previously shown [23] that small uncertainties in fluid properties can result in very large uncertainties in the calculated B-factor. Large uncertainties in B-factor result in correspondingly large uncertainties in Δh_v and result in crude correlative and predictive analyses.

---

[2] See communications by A. B. Bailey (p. 57), F. C. Gilman (p. 58) and M. Sutton (p. 63) at end of Chivers [9] paper.

If we were not attempting to correlate data from pump-to-pump, we could relax our selection criteria. Correlating data for a given pump and fluid at various inlet conditions or for a given pump with different fluids is much less difficult. In the latter two cases, the first selection criterion is not applicable and the second and third criteria are relaxed somewhat because a single test apparatus is used, i.e., the test procedures, data uncertainties, data analysis techniques, experimenter judgments, etc., should be reasonably consistent. The fourth and fifth selection criteria are of vital importance in all correlative work. Selected data from Saleman [16] and Spraker [18] were previously correlated [5] using the simplified expressions reproduced herein. These data were only suitable for fluid-to-fluid correlations and NPSH requirements were generally predicted within the estimated uncertainties of the experimental NPSH data. The predictions are undoubtedly well within the combined uncertainties in pump data and fluid properties data.

After careful study of the NASA-LeRC pump data [4-6, 34-36] and discussion of these data with one of the NASA authors [33], additional selection criteria were imposed.

a) Some of the low ϕ inducer data were rejected because of the 'dips' and 'wiggles' in the ψ - NPSH curves (see figure 4.2). Such data complicate the determination of ΔH_{nc} and the NPSH for prescribed values of ψ'. Because of the difficulty in establishing ψ'_{nc} for some of the higher ϕ data, the higher values of ψ' were not used; i.e., the uncertainty in graphically evaluating NPSH for a specific ψ' is minimized at lower values of ψ'--again, refer to figure 4.2. All inducer data were restricted to values of $\psi' = 0.7$. Values of $\psi' = 0.7$, 0.8, and 0.9 were used for the impeller data.

b) All NPSH data were selected so that there was minimal possibility of the existence of vapor in the pump inlet liquid, see figure 4.2.

c) In the data reported by NASA-LeRC, it is implied that $K_{c,min}$ does not vary with T_o or N, but is a function of ϕ only at constant values of ψ'. In pump-to-pump correlations it is convenient for $K_{c,min}$ to be a function of but two parameters, ϕ and ψ'. Thus, it was imposed that $K_{c,min} \approx$ constant (± 20 percent) for fixed values of ϕ and ψ', at all values of T_o and N for each impeller and each inducer. All of the NASA pump data met this criterion except for the 78° inducer data [36]. The 78° inducer data had variations in calculated $K_{c,min}$ that varied by 300 to 400 percent. It is felt that this selection criterion reflects on the internal consistency of the cavitation data for each piece of pumping equipment; therefore, the performance data for the 78° inducer were rejected. The apparent inconsistency in these 78° inducer data may possibly be attributable to the low cascade solidity (1.856) of this inducer. A solidity ≥ 2.0 to 2.5 improves suction performance and tends to counteract cavitation-induced oscillations--see Jakobsen [45].

The pump impeller and inducer data selected from the NASA publications [4-6, 34-36] are listed in table 4.3. These data are correlated herein. Geometrical details of the NASA pump equipment are summarized in table 4.4 and photographs of the NASA pump impellers and inducers are shown on figure 4.3.

4.5 Correlation of Pump Impeller and Inducer Data

After fully evaluating the NBS stationary-body data, it was decided that the following two equations should be used to correlate the NASA-LeRC hydrogen pump data:

$$\frac{B}{B_{ref}} = \left(\frac{\alpha_{ref}}{\alpha}\right)^{1.0} \left(\frac{V_o}{V_{o,ref}}\right)^{0.8} \left(\frac{\ell}{\ell_{ref}}\right)^{0.3} \left(\frac{D}{D_{ref}}\right)^{0.6} \; ; \quad (4-3)$$

Table 4.3   Selected data from NASA-LeRC hydrogen pump experiments.

PUMP	DATA TEST POINT	T_o (K)	N (rpm)	ψ'	ϕ	NPSHE (m)	$\bar{K}_{c,min}$	$\bar{S}_c$
IMPELLER A	1 *	20.7	25000	0.90	0.225	29.3	1.895	2.004
	2 *	20.7	27600	0.90	0.225	39.9	1.895	2.004
	3	20.6	30000	0.90	0.225	53.0	1.895	2.004
	4 *	20.7	25000	0.80	0.225	24.4	1.611	2.171
	5 *	20.7	27600	0.80	0.225	33.5	1.611	2.171
	6	20.6	30000	0.80	0.225	45.7	1.611	2.171
	7 *	20.7	25000	0.70	0.225	21.3	1.402	2.312
	8 *	20.7	27600	0.70	0.225	29.6	1.402	2.312
	9	20.6	30000	0.70	0.225	40.8	1.402	2.312
	10	20.6	25000	0.90	0.245	35.4	1.842	1.868
	11	20.4	27700	0.90	0.245	52.1	1.842	1.868
	12	20.6	30100	0.90	0.245	63.1	1.842	1.868
	13	20.4	25000	0.80	0.245	30.8	1.653	1.966
	14	20.4	27700	0.80	0.245	46.3	1.653	1.966
	15	20.6	30100	0.80	0.245	54.9	1.653	1.966
	16	20.6	25000	0.70	0.245	28.7	1.163	2.312
	17	20.4	27700	0.70	0.245	42.1	1.163	2.312
	18	20.6	30100	0.70	0.245	50.3	1.163	2.312
	19	20.8	25100	0.90	0.260	58.2	2.231	1.597
	20	20.7	27750	0.90	0.260	77.7	2.231	1.597
	21	20.7	30300	0.90	0.260	96.3	2.231	1.597
	22	20.8	25100	0.80	0.260	51.8	2.079	1.656
	23	20.7	27750	0.80	0.260	69.2	2.079	1.656
	24	20.7	30300	0.80	0.260	87.8	2.079	1.656
IMPELLER B	25 *	20.7	8815	0.90	0.440	93.0	5.917	0.533
	26 *	20.8	11770	0.90	0.440	190.5	5.917	0.533
	27	20.9	14600	0.90	0.440	319.7	5.917	0.533
	28 *	20.7	8815	0.80	0.440	84.1	5.650	0.549
	29 *	20.8	11770	0.80	0.440	176.2	5.650	0.549
	30	20.9	14600	0.80	0.440	300.8	5.650	0.549
	31 *	20.7	8815	0.70	0.440	79.2	5.477	0.560
	32 *	20.8	11770	0.70	0.440	168.6	5.477	0.560
	33	20.9	14600	0.70	0.440	289.6	5.477	0.560

* Denotes reference data used to compute the results recorded in Tables 4.6 and 4.7.

Table 4.3 Selected data from NASA-LeRC hydrogen pump experiments. (Concluded)

| PUMP	DATA TEST POINT	T_0 (K)	N (rpm)	ψ'	ϕ	$NPSH_E$ (m)	$\bar{K}_{c,min}$	$\bar{S}_c$
INDUCER A	34	15.5	20000	0.70	0.065	11.6	3.060	5.378
	35	17.2	20000	0.70	0.065	6.4	3.060	5.378
	36	15.5	20000	0.70	0.070	14.6	3.091	4.966
	37 ✱	17.2	20000	0.70	0.070	10.1	3.091	4.966
	38	15.5	20000	0.70	0.073	16.6	3.175	4.723
	39	17.2	20000	0.70	0.073	12.6	3.175	4.723
	40 ✱	18.9	20000	0.70	0.073	5.0	3.175	4.723
	41	15.5	20000	0.70	0.075	19.2	3.420	4.374
	42	17.2	20000	0.70	0.075	15.2	3.420	4.374
	43	18.9	20000	0.70	0.075	7.6	3.420	4.374
INDUCER B	44	17.2	25000	0.70	0.105	42.0	2.751	3.533
	45	18.9	25000	0.70	0.105	26.0	2.751	3.533
	46 ✱	17.2	25000	0.70	0.110	52.0	3.009	3.209
	47	18.9	25000	0.70	0.110	36.0	3.009	3.209
	48	17.2	25000	0.70	0.115	61.0	3.154	2.988
	49	18.9	25000	0.70	0.115	45.0	3.154	2.988
	50	17.2	30000	0.70	0.105	68.0	2.737	3.544
	51	18.9	30000	0.70	0.105	52.0	2.737	3.544
	52	20.3	30000	0.70	0.105	33.0	2.737	3.544
	53	17.2	30000	0.70	0.110	82.0	3.038	3.193
	54	18.9	30000	0.70	0.110	67.0	3.038	3.193
	55	20.3	30000	0.70	0.110	48.0	3.038	3.193
	56	21.1	30000	0.70	0.110	32.0	3.038	3.193
	57	17.2	30000	0.70	0.115	95.0	3.214	2.963
	58 ✱	18.9	30000	0.70	0.115	80.0	3.214	2.963
	59	20.3	30000	0.70	0.115	63.0	3.214	2.963
	60	21.1	30000	0.70	0.115	45.0	3.214	2.963

✱ Denotes reference data used to compute the results recorded in Tables 4.6 and 4.7.

Table 4.4 Geometrical details of the NASA-LeRC pump impellers and inducers.

Geometrical Parameter	Impeller A	Impeller B
Main (inlet) blade tip $\angle$ (from axial direction = $90° - \beta$), deg	71.3	68
β = main blade tip $\angle$ (from circumferential direction) deg	18.7	22
$\beta_1 = \beta/2$ = fairing $\angle$ at tip, deg	9.35	11
n = number of main blades	12	7
n_{ps} = number of primary splitter vanes	12	7
n_{ss} = number of secondary splitter vanes	24	14
t_b = blade thickness, cm	0.200	0.158
C_t = main blade chord length at tip, cm	5.842	5.842
C_h = main blade chord length at hub, cm	6.287	7.366
C_{ub} = unblocked chord length at tip, cm	1.397	3.471
C_{st} = modified cascade solidity at tip [$\equiv C_t/C_{ub}$]	4.182	1.683
Impeller axial length, cm	3.350	5.319
D_t = main blade tip diameter, cm	6.782	9.804
$D_{t,ps}$ = tip diameter of primary splitter, cm	7.417	11.532
$D_{t,ss}$ = tip diameter of secondary splitter, cm	8.232	14.539
D_h = main blade hub diameter, cm	4.763	7.000
$D_{h,ps}$ = hub diameter of primary splitter, cm	6.194	8.941
$D_{h,ss}$ = hub diameter of secondary splitter, cm	7.811	13.381
D_D = overall (discharge) diameter of impeller, cm	11.557	18.887
D_h/D_t = main blade hub-to-tip ratio	0.702	0.714

Table 4.4 Geometrical details of the NASA-LeRC pump impellers and inducers. (Concluded)

Geometrical Parameter	Inducer A	Inducer B
Blade tip helix ∢ (from axial direction = 90° - β), deg	84	80.6
β = blade tip ∢ (from circumferential direction), deg	6	9.4
β_1 = blade leading edge fairing ∢, deg	3	4.7
n = number of blades	3	3
t_b = tip blade thickness, cm	0.170	0.254
hub blade thickness, cm	0.254	0.381
Peripheral extent (PE) of blades, deg	440	280
C_t = blade chord length at tip, cm	48.89 [a]	31.33 [a]
C_h = blade chord length at hub, cm	24.30 [b]	15.59 [b]
C_{ub} = unblocked blade chord length at tip, cm	13.189 [c]	13.069 [c]
C_{st} = modified cascade solidity at tip	3.707 [d]	2.397 [d]
Inducer axial length, cm	5.08	5.08
D_t = rotor tip diameter, cm	12.664	12.649
D_h = rotor hub diameter, cm	6.294	6.294
D_h/D_t = hub-to-tip ratio	0.497	0.498
Calculated radial tip clearance @ 20 K, cm	0.064	0.064
Ratio of tip clearance to blade height	0.020	0.020

a --- $C_t = [(PE/360)\pi D_t]/\cos \beta$

b --- $C_h = [(PE/360)\pi D_h]/\cos \beta$

c --- $C_{ub} = (\pi D_t/n) \cos \beta$

d --- $C_{st} = C_t/C_{ub}$
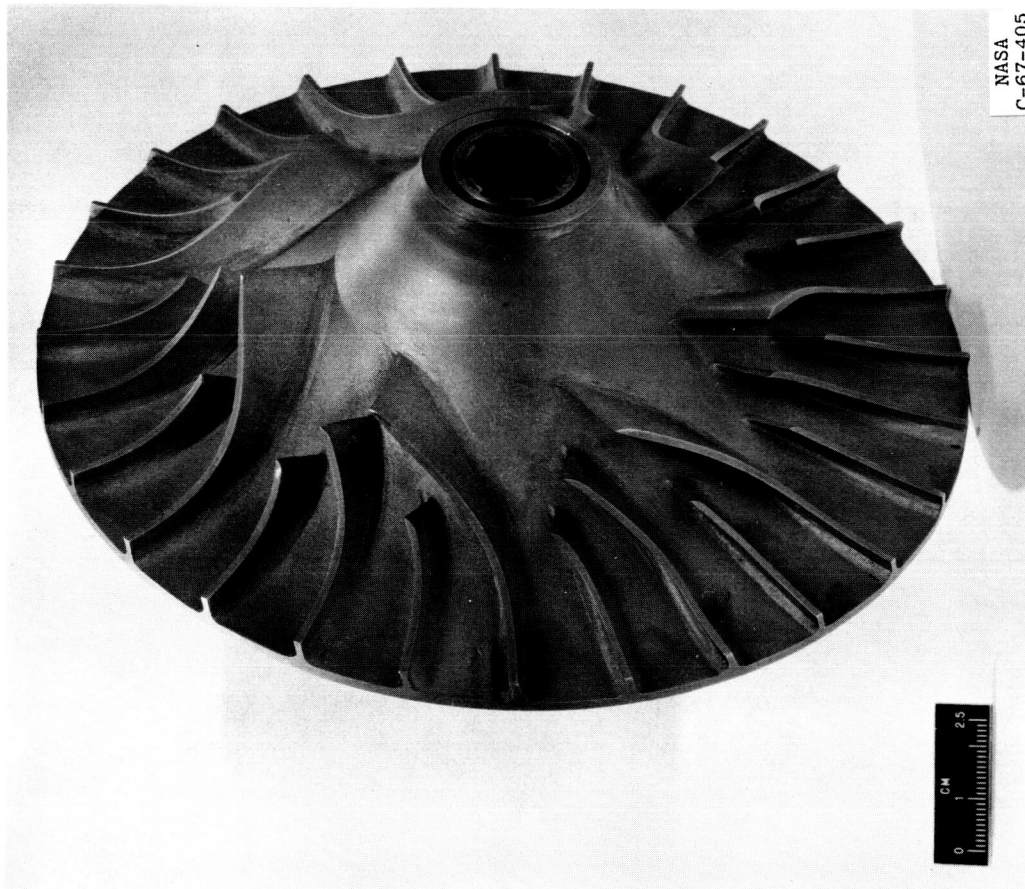
NASA
C-67-405

b) Centrifugal Impeller B
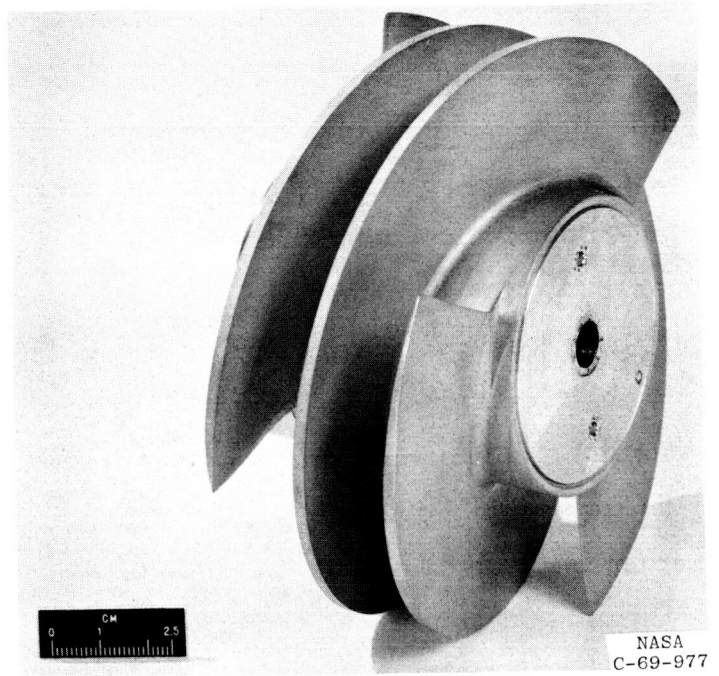**($\beta = 22°$)**
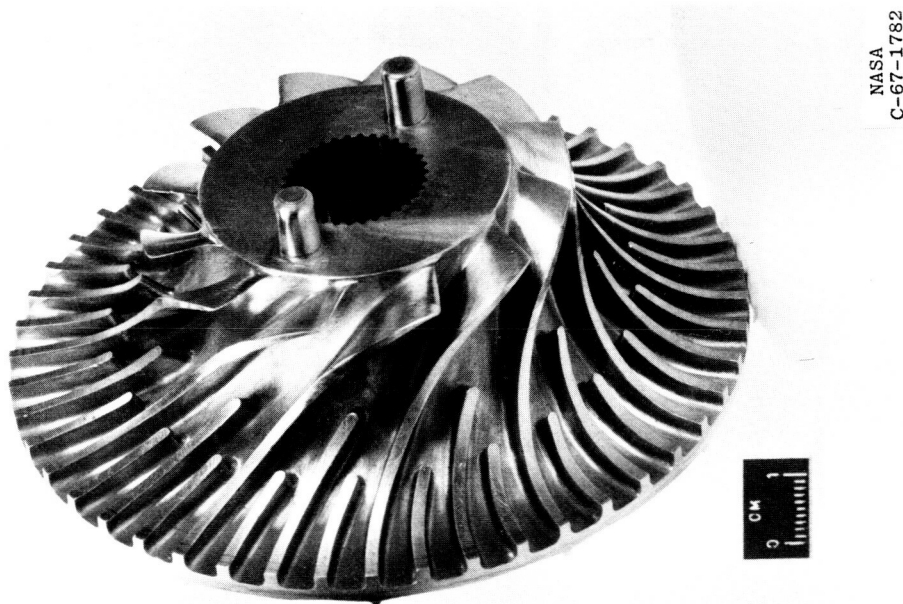
NASA
C-67-1782
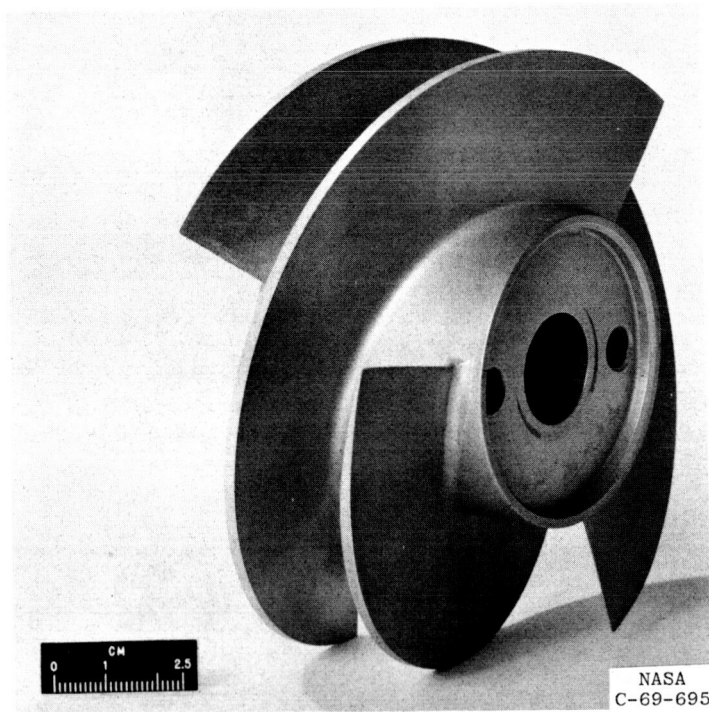
a) Centrifugal Impeller A
($\beta = 18.7°$)

Figure 4.3   Photographs of the NASA-LeRC pump impellers and inducers.

35

c) Helical Inducer A
($\beta = 6°$).

d) Helical Inducer B
($\beta = 9.4°$).

e) Helical Inducer C
($\beta = 12°$).

Figure 4. 3 (Concluded).

36

$$\frac{B}{B_{ref}} = \left(\frac{MTWO}{MTWO_{ref}}\right)^{0.51} \left(\frac{\ell}{\ell_{ref}}\right)^{0.28} \left(\frac{D}{D_{ref}}\right)^{0.43} . \quad (4-4)$$

To show true size effect [22], the ℓ and D terms may be combined to form the dimensionless ratio, ℓ/D, as follows:

$$\frac{B}{B_{ref}} = \left(\frac{\alpha_{ref}}{\alpha}\right)^{1.0} \left(\frac{V_o}{V_{o,ref}}\right)^{0.8} \left(\frac{\ell/D}{(\ell/D)_{ref}}\right)^{0.3} \left(\frac{D}{D_{ref}}\right)^{0.9} ;$$

$$(4-5)$$

$$\frac{B}{B_{ref}} = \left(\frac{MTWO}{MTWO_{ref}}\right)^{0.51} \left(\frac{\ell/D}{(\ell/D)_{ref}}\right)^{0.28} \left(\frac{D}{D_{ref}}\right)^{0.71} . \quad (4-6)$$

The ℓ/D ratio is used in a wide variety of geometric scaling problems, and the true 'size effect' is indicated by the value of the exponent on the D term; i.e., for the same ℓ/D ratio the size effect is mathematically represented by $(D/D_{ref})^{0.9}$ or $(D/D_{ref})^{0.71}$ in eqs (4-5) and (4-6).

The first three exponentiated terms of eq (4-5) are those used by Moore and Ruggeri [3-6]--the D term was derived from the NBS stationary-body data. Thus, eq (4-5) is used herein to provide continuity with the correlative/predictive work of Moore and Ruggeri and to provide a comparison of eq (4-5) and eq (4-6) when used to correlate pump data. Equation (4-6) was far superior to the mathematical form given in eq (4-5) for the correlation of stationary-body data; therefore, eq (4-6) was expected to excel when correlating pump data with these two equations. The results given herein confirmed this reasoning.

To apply eq (4-5) or eq (4-6) to the correlation of pump data, we must relate B to Δh_v and then relate Δh_v to the NPSH requirements of each pump. Thus, an additional mathematical relationship is required and obtained from definition of cavitation parameters. First the cavitation parameter is defined [4] in terms of the minimum cavity pressure by the relation

37

$$K_{c,min} = \frac{h_o - h_{c,min}}{V_o{}^2/2g_c} = K_v + \frac{\Delta h_v}{V_o{}^2/2g_c} \, , \qquad (4\text{-}7)$$

where K_v is the conventional cavitation parameter defined by

$$K_v = \frac{h_o - h_v}{V_o{}^2/2g_c} \, . \qquad (4\text{-}8)$$

It is apparent from eq (4-7) that $K_{c,min} = K_v$ when $\Delta h_v = 0$ and by definition we have replaced h_v in eq (4-8) with $h_{c,min}$ in eq (4-7). Next, we take the definition of

$$NPSH = h_o + \frac{V_o{}^2}{2g_c} - h_v \, . \qquad (4\text{-}9)$$

Combining eq (4-8) and eq (4-9), we get

$$K_v = \left[\left(\frac{2g_c}{V_o{}^2} \right) NPSH \right] - 1 \, . \qquad (4\text{-}10)$$

Then eq (4-7) and eq (4-10) may be combined to form

$$\left(1 + K_{c,min} \right) \frac{V_o{}^2}{2\,g_c} = \left(NPSH + \Delta h_v \right) . \qquad (4\text{-}11)$$

Equation (4-11) indicates the relationship that must exist between NPSH and the cavitating pressure coefficient, $K_{c,min}$; it also provides the framework for the second required mathematical expression. We may rewrite eq (4-11) in terms of pump parameters as

$$\left(1 + K_{c,min} \right) \frac{(\phi ND_t)^2}{2\,g_c} = \left(NPSH + \Delta h_v \right) , \qquad (4\text{-}12)$$

where $V_o = \phi ND_t$. Expressing eq (4-12) in terms of reference data, we obtain the desired expression

$$\frac{(1 + K_{c,min})}{(1 + K_{c,min})_{ref}} \left(\frac{\phi ND_t}{(\phi ND_t)_{ref}}\right)^2 = \frac{(NPSH + \Delta h_v)}{(NPSH + \Delta h_v)_{ref}} . \quad (4-13)$$

Equation (4-13) may now be paired with eq (4-5) or eq (4-6) to form the equation pairs needed to correlate the pump data. Equation (4-5) and eq (4-13) constitute our first equation pair

$$\left\{ \begin{array}{l} \dfrac{(1 + K_{c,min})}{(1 + K_{c,min})_{ref}} \left(\dfrac{\phi ND_t}{(\phi ND_t)_{ref}}\right)^2 = \dfrac{(NPSH + \Delta h_v)}{(NPSH + \Delta h_v)_{ref}} \\[4ex] \dfrac{B}{B_{ref}} = \left(\dfrac{\alpha_{ref}}{\alpha}\right)^{1.0} \left(\dfrac{\phi ND_t}{(\phi ND_t)_{ref}}\right)^{0.8} \left(\dfrac{\ell/D_t}{(\ell/D_t)_{ref}}\right)^{0.3} \left(\dfrac{D_t}{D_{t,ref}}\right)^{0.9} \end{array} \right\}$$

$$(4-14)$$

where D_t replaces the characteristic dimension D in eq (4-5) and $V_o = \phi ND_t$.

Equations (4-14) differ from those formulated by Ruggeri and Moore [3-6] only in the value of the exponent on the D_t term in the second equation. To assure dynamic and geometric similarity of cavitating flow, eqs (4-14) were restricted [3-6] to a single pump. Physical reasoning [4] and venturi tests [46] indicated that $K_{c,min}$ could be expected to vary with ϕ for any specific pump. Subsequent pump experiments [4-6] substantiated this idea. Variation in ϕ causes a change in flow incidence angle. Therefore, variation in ϕ is analogous to an actual change in blade geometry for a specific pump and results

39

in a different $K_{c,min}$ for each value of ϕ. Because $K_{c,min}$ was not predictable prior to testing, Moore and Ruggeri simplified eqs (4-14) by specifying that constant values of $K_{c,min}$, ϕ, and ψ' be used to predict cavitating performance of a given pump. Constant ψ' relates to cavity volume and constant values of ℓ/D_t as will be discussed later in this report. Holding $K_{c,min}$, ϕ, ψ', and pump geometry constant, we obtain the simplified equation pair used with good success by Moore and Ruggeri [3-6]:

$$
\left\{
\begin{array}{c}
\left(\dfrac{N}{N_{ref}}\right)^2 = \dfrac{(NPSH + \Delta h_v)}{(NPSH + \Delta h_v)_{ref}} \\[4mm]
\dfrac{B}{B_{ref}} = \left(\dfrac{\alpha_{ref}}{\alpha}\right)^{1.0} \left(\dfrac{N}{N_{ref}}\right)^{0.8}
\end{array}
\right\}
\qquad (4-15)
$$

The third equation pair is obtained by using eq (4-6) and eq (4-13):

$$
\left\{
\begin{array}{c}
\dfrac{(1 + K_{c,min})}{(1 + K_{c,min})_{ref}} \left(\dfrac{\phi ND_t}{(\phi ND_t)_{ref}}\right)^2 = \dfrac{(NPSH + \Delta h_v)}{(NPSH + \Delta h_v)_{ref}} \\[4mm]
\dfrac{B}{B_{ref}} = \left(\dfrac{MTWO}{MTWO_{ref}}\right)^{0.51} \left(\dfrac{\ell/D_t}{(\ell/D_t)_{ref}}\right)^{0.28} \left(\dfrac{D_t}{D_{t,ref}}\right)^{0.71}
\end{array}
\right\}
$$

$$(4-16)$$

Referring to eqs (4-16), we note that the first equation is derived from basic definitions and is not restricted to a singular pump geometry; therefore, the first equation of (4-16) may be extended to predict cavitating performance from one pump to another if all of the parameters in this equation are known. The next section of this

report elaborates on this topic. For the second equation in (4-16) to be applicable to varying pump geometries, we must satisfy ourselves that the basic cavity shapes and heat and mass transfer phenomena do not vary markedly from one pump to another. The cavity shape data obtained in our stationary-body tests [22] and those from Rouse and McNown [29] indicate that cavities formed on a wide variety of hydrodynamic bodies are generally parabolic. Also, the exponent data for the second equation in (4-16) are remarkably consistent for the various stationary-bodies tested in this study (see table 4.2). This consistency of exponent values indicates that the heat and mass transfer processes associated with cavitation [21] do not vary appreciably for these hydrodynamic bodies. Thus, it appears that the second equation of (4-16) is equally applicable to varying pump geometries provided that this equation is initially evaluated from experimental data where there exists significant variation in body geometries. It is felt that this latter criterion is met by using the results of the VHO data correlated herein.

Arguments similar to those presented above may be advanced in favor of using eqs (4-14) to correlate cavitating performance from pump to pump; however, the exponent data for the second equation of (4-14) are relatively inconsistent for different body geometries (see table 4.2), and these arguments are less convincing. For a specific pump geometry, equation pairs (4-14) and (4-16) are equally applicable. Equations (4-14) are applied herein (to specific pumps and to varying pump geometries) to provide a comparison of proven predictive expressions with the improved expressions given in eqs (4-16).

Equations (4-14) and (4-16) were used to correlate the NASA-LeRC pump data. The correlative results are summarized in tables 4.5 through 4.7 and are discussed in detail in the following section of this report. Exact computational procedures with numerical examples are illustrated for eqs (4-16) in appendix A. The detailed illustrations [4] for use of eqs (4-15) may also be helpful to the reader.

41

Table 4.5 Correlation of NASA-LeRC hydrogen pump data; ψ', ϕ, and pump geometry are held constant but N and T_o are varied. Reference data by cyclic permutation.

MEAN PERCENT ERROR (MPE)* in PREDICTED~ NPSH using EQUATIONS (4-14) and (4-16)

PUMP	ψ'	ϕ	MPE obtained using		NTPP
			Eqs.(4-14)	Eqs.(4-16)	
IMPELLER A	0.9	0.225	1.39	2.18	3
	0.9	0.245	1.19	2.87	3
	0.9	0.260	1.15	1.44	3
	0.8	0.225	3.32	4.14	3
	0.8	0.245	6.54	9.30	3
	0.8	0.260	1.68	1.25	3
	0.7	0.225	3.89	4.91	3
	0.7	0.245	1.59	5.50	3
IMPELLER B	0.9	0.440	2.78	2.95	3
	0.8	0.440	4.05	4.21	3
	0.7	0.440	4.08	4.25	3
INDUCER A	0.7	0.0725	11.03	4.78	3
	0.7	0.0750	7.69	3.35	3
INDUCER B	0.7	0.105	21.27	11.56	30
	0.7	0.110	29.43	9.18	60
	0.7	0.115	30.16	6.31	60

Equation Pair	OMPE**
Eqs. (4-16)	7.56
Eqs. (4-14)	23.09

* MPE $= \left[\sum\left\{|NPSH_P - NPSH_E|(100/NPSH_E)\right\}\right] / NTPP$

** OMPE $= \left[\sum\left\{\sum\left\{(MPE)NTPP\right\}\right\}\right] / \sum(NTPP)$, where NTPP = number of test points predicted and the subscripts P and E denote predicted and experimental, respectively.

~ These tedious and sometimes arduous computations were computer-coded and supplied by William R. Parrish.

Table 4.6 Correlation of NASA-LeRC hydrogen pump data: ψ' is held constant but pump geometry, ϕ, N and T_o are varied; D_t = characteristic dimension. Reference data are indicated in table 4.3.

MEAN PERCENT ERROR (MPE)* in PREDICTED✙ NPSH using EQUATIONS (4-14) and (4-16)

PREDICTED \ REFERENCE →	IMPELLER A, $\psi'=0.9$ Eqs.	MPE	IMPELLER A, $\psi'=0.8$ Eqs.	MPE	IMPELLER A, $\psi'=0.7$ Eqs.	MPE	IMPELLER B, $\psi'=0.9$ Eqs.	MPE	IMPELLER B, $\psi'=0.8$ Eqs.	MPE	IMPELLER B, $\psi'=0.7$ Eqs.	MPE	INDUCER A, $\psi'=0.7$ Eqs.	MPE	INDUCER B, $\psi'=0.7$ Eqs.	MPE
IMPELLER A $\psi'=0.9$	(4-16) (4-14)	4.89 8.36 (7)=NTPP					(4-16) (4-14)	9.62 11.92 (9)								
IMPELLER A $\psi'=0.8$			(4-14) (4-16)	4.64 4.96 (7)					(4-16) (4-14)	15.98 21.89 (9)						
IMPELLER A $\psi'=0.7$					(4-14) (4-16)	7.11 13.73 (4)					(4-16) (4-14)	37.70 41.01 (6)	(4-16) (4-14)	8.93 22.61 (6)	(4-16) (4-14)	8.95 11.84 (6)
IMPELLER B $\psi'=0.9$	(4-16) (4-14)	2.56 4.46 (3)					(4-14) (4-16)	1.99 2.09 (1)								
IMPELLER B $\psi'=0.8$			(4-16) (4-14)	4.09 5.38 (3)					(4-14) (4-16)	2.80 2.91 (1)						
IMPELLER B $\psi'=0.7$					(4-16) (4-14)	5.34 6.81 (3)					(4-14) (4-16)	2.75 2.90 (1)	(4-16) (4-14)	5.73 8.13 (3)	(4-16) (4-14)	5.66 9.40 (3)
INDUCER A $\psi'=0.7$					(4-16) (4-14)	9.55 13.54 (10)					(4-14) (4-16)	20.13 35.78 (10)	(4-16) (4-14)	9.77 15.41 (8)	(4-16) (4-14)	8.37 24.52 (10)
INDUCER B $\psi'=0.7$					(4-14) (4-16)	8.34 10.70 (17)					(4-16) (4-14)	5.59 11.77 (17)	(4-16) (4-14)	11.72 12.29 (17)	(4-16) (4-14)	12.93 17.38 (15)

Equation Pair	OMPE**
Eqs. (4-16)	11.65
Eqs. (4-14)	14.22

* $\text{MPE} = \left[\sum \left\{ |NPSH_P - NPSH_E| (100/NPSH_E) \right\} \right] / NTPP$

** $\text{OMPE} = \left[\sum \left\{ (MPE)\, NTPP \right\} \right] / \sum (NTPP)$, where NTPP = number of test points predicted and the subscripts P and E denote predicted and experimental, respectively.

✙ These tedious and sometimes arduous computations were computer-coded and supplied by William R. Parrish.

43

Table 4.7 Correlation of NASA-LeRC hydrogen pump impeller data: ψ' is held constant but pump geometry, ϕ, N and T_Q are varied; D_{m2} = characteristic dimension. Reference data are indicated in table 4.3.

MEAN PERCENT ERROR (MPE)* in PREDICTED* NPSH using EQUATIONS (4-14) and (4-16)

REFERENCE → / ↓ PREDICTED	IMPELLER A						IMPELLER B						INDUCER A		INDUCER B	
	$\psi'=0.9$		$\psi'=0.8$		$\psi'=0.7$		$\psi'=0.9$		$\psi'=0.8$		$\psi'=0.7$		$\psi'=0.7$		$\psi'=0.7$	
	Eqs.	MPE	Eqs.	MPE	Eqs.	MPE	Eqs.	MPE	Eqs.	MPE	Eqs.	MPE	Eqs.	MPE	Eqs.	MPE
IMPELLER A $\psi'=0.9$							(4-16) (4-14)	4.18 8.70 (9)								
IMPELLER A $\psi'=0.8$									(4-16) (4-14)	7.33 13.82 (9)						
IMPELLER A $\psi'=0.7$											(4-16) (4-14)	26.24 30.42 (6)				
IMPELLER B $\psi'=0.9$	(4-16) (4-14)	1.37 2.32 (3)=NTPP														
IMPELLER B $\psi'=0.8$			(4-16) (4-14)	2.88 3.83 (3)												
IMPELLER B $\psi'=0.7$					(4-16) (4-14)	3.53 5.21 (3)										
INDUCER A $\psi'=0.7$																
INDUCER B $\psi'=0.7$																

* MPE = $\left[\sum \left\{ |NPSH_P - NPSH_E|(100/NPSH_E) \right\} \right] / NTPP$

** OMPE = $\left[\sum \left\{ (MPE)\,NTPP \right\} \right] / \sum (NTPP)$, where NTPP = number of test points predicted and the subscripts P and E denote predicted and experimental, respectively.

~ These tedious and sometimes arduous computations were computer-coded and supplied by William R. Parrish.

For pump designers, it is instructive to demonstrate the relationship between $K_{c, min}$ and the cavitating suction specific speed S_c. First, we note that the noncavitating suction specific speed

$$S_{nc} = (NQ^{1/2}) / (NPSH)^{3/4} . \qquad (4-17)$$

By replacing NPSH in eq (4-17) with $(NPSH + \Delta h_v)$ as we did in making the transition from K_v in eq (4-10) to $K_{c, min}$ in eq (4-11), we obtain

$$S_c = (NQ^{1/2}) / (NPSH + \Delta h_v)^{3/4} . \qquad (4-18)$$

Combining eq (4-11) and (4-18) and substituting $Q = A_o V_o$, $V_o = \phi ND_t$, and $A_o = (\pi D_o^2) / 4$ yields

$$S_c = \frac{\left[(\pi/4)^{1/2} (2g_c)^{3/4} \right] (D_o/D_t)}{\phi (1 + K_{c, min})^{3/4}} . \qquad (4-19)$$

The significance of holding ϕ, $K_{c, min}$ and pump geometry constant as in the development of eqs (4-15) is now apparent--S_c is also held constant. Holding S_c = constant implies similar suction performance which is precisely the optimum condition for application of eqs (4-14) and (4-16).

If preferred, we may now use eq (4-19) to rewrite eq (4-13) in terms of S_c. Eliminating $K_{c, min}$ in combining these two equations produces

$$\left(\frac{(S_c \phi)_{ref}}{S_c \phi} \right)^{4/3} \left(\frac{D_o/D_t}{(D_o/D_t)_{ref}} \right)^{4/3} \left(\frac{\phi ND_t}{(\phi ND_t)_{ref}} \right)^2 = \frac{(NPSH + \Delta h_v)}{(NPSH + \Delta h_v)_{ref}}$$

$$(4-20)$$

Equation (4-20) may now be paired with eq (4-5) or eq (4-6) to form
the desired correlative/predictive expressions. These equation pairs
will produce mathematical results that are identical to those obtained
from eqs (4-14) and (4-16), respectively. Again, a method of evaluating
S_c (or $K_{c,min}$) is needed in order to apply these predictive expressions
to varying pump geometries.

4.6 Discussion of Pump Impeller and Inducer Data

Correlation of the NASA-LeRC pump data with eqs (4-14) and
(4-16) requires $K_{c,min}$ vs ϕ data for each pump. $K_{c,min}$ was calculated
for each value of ϕ and for each pump using eq (4-14) or eq (4-16) and
the NASA-LeRC experimental data. The procedure for calculating
$K_{c,min}$ and corresponding values of S_c from experimental data is
described in appendix A. Calculated values of $K_{c,min}$ and S_c are
given in table 4.3. In practice, $K_{c,min}$ (or S_c) will be unknown prior
to pump testing; therefore, use of eqs (4-14) or (4-16) for predictive
purposes will require an independent method of estimating $K_{c,min}$.
Potential techniques for determining $K_{c,min}$ (or S_c) are suggested in
this report.

Cavity lengths may be calculated if cavity vapor volumes and
characteristic dimensions of each pump are known; however, we have
insufficient knowledge concerning the extent of cavity vapor volumes
within pump blade passages and must take ℓ/D_t = constant in eqs (4-14)
and (4-16). This constraint is defensible only for <u>similar</u> cavity shapes;
therefore, it is considered valid for homologous pumps but perhaps
inaccurate for dissimilar pumps. As a result of increased vapor block-
age, pump head will decrease as cavities grow within the blade passages;
thus ψ' must be functionally related to $\mathcal{V}_v$ for all pumps. ψ' decreases as
$\mathcal{V}_v$ increases and these trends lead us to suggest a simple functional
relationship

$$\mathcal{V}_v \propto 1 - \psi'. \tag{4-21}$$

Because $\mathcal{V}_v$ is mathematically related to ℓ/D_t we can also assert that

ψ' is a function of ℓ/D_t. Obviously these functions, $\mathcal{V}_v = f(\psi')$, $\mathcal{V}_v = f(\ell/D_t)$ and $\psi' = f(\ell/D_t)$, may differ from one pump to another; however, holding $\psi' = $ constant seems sufficient to assure that $\ell/D_t = $ constant for similar cavity shapes in similar pumps. We will also have to be content with this constraint for pump-to-pump correlations, even though we are fully aware that it may be inappropriate. Fortunately, ℓ/D_t is a weakly exponentiated term in eqs (4-14) and (4-16) and thereby forgives many weaknesses of the imposed constraint.

The results given in table 4.5 are for the simplified and optimum condition where ψ', ϕ, and $K_{c,min}$ are invariant. These criteria also require that the pump geometry be invariant because each pump was tested over a different range of ϕ's. Thus, the reference data and predictions relate to identical pump geometries as witnessed by the numerical entries along the horizontal lines of table 4.5. These data indicate the suitability of eqs (4-14) and (4-16) for predicting NPSH under the prescribed conditions. All possible pairs of experimental data points were used to establish reference data for each pump--two experimental test points are required to establish reference data (see appendix A)-- and then each set of reference data was used to calculate the mean percent error (MPE) in predicted NPSH. The MPE values reported in table 4.5 are the arithmetic average of all possible permutations of the available reference data. Using a single set of reference data produces results similar to those given in table 4.5 but with less statistical significance. Due to the scarcity of constant ϕ data it was felt that the results shown in table 4.5 were most representative of the available data.

The results given in table 4.5 indicate that eqs (4-14) and (4-16) are quite adequate for correlating the impeller data but that eq (4-16) excels in correlating the inducer data. The overall correlative-predictive results are given in the bottom right-hand corner of this table. The overall success of the predictive expressions is assessed by calculating the overall mean percent error (OMPE) in predicted NPSH,

$$OMPE = \frac{\sum\{(MPE) \ NTPP\}}{\sum (NTPP)} . \qquad (4\text{-}22)$$

Under the prescribed conditions, we could reasonably expect to predict NPSH within about ± 8 percent using eqs (4-16).

Table 4.6 lists the results for pump-to-pump predictions with $\psi' =$ constant; here, appropriate blocks in the table identify the reference and predicted pump geometries. As an example, the use of eqs (4-16) and reference data from impeller A at $\psi' = 0.7$ produces MPE values of 13.73, 5.34, 9.55, and 10.70 in predicting the cavitating performance of impeller A, impeller B, inducer A, and inducer B, respectively. The correlative equations producing the lowest MPE are listed first in each data block within table 4.6. The values of MPE shown in this table were calculated using the reference data identified in table 4.3. These reference data minimized the OMPE for eqs (4-16) and produced nearly optimum results for eqs (4-14). Thus, the predictive results shown in table 4.6 may be considered the best possible using eqs (4-16), and under the most favorable conditions we might predict NPSH within about ± 12 percent (see OMPE for eqs (4-16) in table 4.6). That eqs (4-16) are clearly superior was again demonstrated by also computing the OMPE for all possible permutations of the available reference data. The resultant values of OMPE were 19.92 and 24.44 for eqs (4-16) and (4-14), respectively. Under the conditions prescribed in table 4.6, but using all available reference data, we could expect to predict NPSH within about ± 20 percent using eqs (4-16).

It is interesting that the values of OMPE obtained using eqs (4-14) do not vary much as correlative restraints are relaxed in going from table 4.5 to table 4.6 (using cyclic permutation of reference data the OMPE varies from 23.09 to 24.44). Conversely, the OMPE for eqs (4-16) is much lower when pump geometry is held constant as in table 4.5 (using cyclic permutation of reference data the OMPE varies from 7.56 to 19.92). Direct comparison of the OMPE values in table 4.5 with the

optimum values in table 4.6 is also interesting--the trend exhibited by eqs (4-16) seems the most logical.

In preparing the results shown in tables 4.5 and 4.6, it became apparent that eqs (4-16) dominantly produce the lowest and most consistent values of OMPE for each set of reference data. As the reference data were varied, the individual values of MPE were also most consistent when eqs (4-16) were used. This improved consistency trend is attributed to use of the MTWO parameter in eqs (4-16). Similar results were obtained for the stationary-body data (see table 4.2). These observations, exemplified by the results given in tables 4.5 and 4.6, clearly demonstrate that eqs (4-16) should be used for all future correlative and predictive work.

As expected we obtain the best correlative and predictive results when ψ', ϕ, $K_{c,min}$ and pump geometry are invariant; however, the NPSH predictions are surprisingly good when only ψ is held constant. Careful study of the data in tables 4.5 and 4.6 reveals that there is room for improvement in the formulation of the predictive expressions. In an effort to improve our predictive capabilities, several ideas were explored as explained in the following paragraphs.

Pump designs [14, 45] employ blade relative velocities to good advantage; therefore, w_t was substituted for V_o in formulating eqs (4-16)-- no correlative improvement was gained. Likewise, no improvement resulted from substitution of blade tip chord length (C_t) for D_t in eqs (4-16). Substitution of the modified cascade tip solidity (C_{st}) for ℓ/D_t in eqs (4-16) also failed to improve the NPSH predictions. Cavitation originates at the tips of the main and splitter blades of the impellers. These blades have different radial and axial coordinates, and selection of appropriate characteristic dimensions is complicated. The main blade tip diameters were selected and used herein, but it is recognized that the primary

and secondary splitter blades also contribute to the overall cavitation performance of equipment.

Accordingly, other characteristic impeller and inducer dimensions were formulated and substituted, in turn, for D_t in eqs (4-14) and (4-16). D_D, D_{m1}, D_{m2}, and D_{m3} were calculated (see table 4.8) and sequentially substituted for D_t: All of these D's were superior to D_t in the impeller-to-impeller correlations. D_{m2} consistently produced the lowest values of MPE as recorded in table 4.7--identical reference data are used in tables 4.6 and 4.7 so that the results shown in these two tables are directly comparable. D_t was generally superior in all other correlations where the inducer data were involved, i.e., in inducer-to-impeller, inducer-to-inducer, or impeller-to-inducer correlations. Because the latter groups comprise the bulk of the pump data, D_t provided the best overall predictions; i.e., D_t produced the lowest values of OMPE. For impeller-to-impeller correlations the future use of D_{m2} is suggested. Better correlative results might possibly be obtained by selection of some other characteristic impeller dimension.

Inducer suction performance is characterized [45] by the ratio θ_1/β, where $\theta_1 = (\tan^{-1}\phi - \beta/2)$ and β is the blade angle. As shown in section 5.2 of this report, θ_2/β can also be considered an important parameter in the analysis of blade cavitation-- $\theta_2 = (\tan^{-1}\phi - \beta)$. For small values of ϕ and β these two parameters, θ_1/β and θ_2/β, are analogous to the normalized ϕ parameter $(\phi/\tan(\beta/2))$ used by Moore and Meng [6]. Attempts to correlate the pump impeller and inducer data at constant values of θ_1/β and/or θ_2/β were disappointing--better results were obtained by unrestricted variation of ϕ as recorded in table 4.6.

Table 4.8 Numerical values for potential characteristic dimensions of pump impellers and inducers.

Pump	D_t	D_D	D_{m1}	D_{m2}	D_{m3}
Impeller A	6.782 cm	11.557 cm	5.860 cm	7.690 cm	7.242 cm
Impeller B	9.804	18.887	8.518	12.766	11.932
Inducer A	12.664	12.664	10.000	- - -	- - -
Inducer B	12.649	12.649	9.990	- - -	- - -

Efforts to improve the pump correlations by using different sets of exponents from table 4.2 were also mostly unsuccessful. Equations (4-14) were equipped with the VHO exponent data from line 8 of table 4.2 and eqs (4-16) were evaluated using the ogive exponent data from line 3 of table 4.2. The latter approach is only slightly inferior to the use of eqs (4-16) as formulated, i.e., when equipped with the VHO exponents from line 4 of table 4.2. This result was anticipated because the exponent data for the ogives and VHO were reasonably consistent. Under the conditions specified in table 4.5, NPSH predictions were improved by equipping eqs (4-14) with the exponent data from line 8 of table 4.2. The use of $(V_o)^{0.11}$, etc., with eqs (4-14) is equivalent to stating that $B \approx B_{ref}$ or $B \approx$ constant when ψ', ϕ, $K_{c,min}$ and pump geometry are held constant. Equations (4-14) with B = constant produced an OMPE of about $\pm$ 10 percent under table 4.5 conditions; however, the OMPE under table 4.6 conditions was drastically increased by holding B constant.

These findings are significant because it appears that the simplified predictive techniques--correlative restraints specified in table 4.5 and use of eqs (4-14)--proposed by Moore and Ruggeri [3-5] can be improved by merely using the definition of $K_{c,min}$ and holding B constant,

$$\left\{ \left(\frac{N}{N_{ref}} \right)^2 = \frac{\left(NPSH + \Delta h_v \right)}{\left(NPSH + \Delta h_v \right)_{ref}} \atop B = B_{ref} = \text{constant} \right\} .$$

(4-23)

Much better results are obtained in all cases by the use of eqs (4-16).

5. POTENTIAL METHODS OF PREDICTING $K_{c,min}$

All of the pump NPSH predictions presented in table 4.6 are based on the premise that $K_{c,min}$ (or S_c) can be estimated without the benefit of pump test data for each specific pump. This section suggests potential techniques for estimating $K_{c,min}$.

5.1 Estimation of $K_{c,min}$ from C_p^v Data

(Pump experiments are not required)

Recognizing that $K_{c,min}$ will vary with ψ' and may vary with ϕ, we will initially settle for rough estimates of $K_{c,min}$; therefore, values of $\overline{K}_{c,min}$ at mean values of ψ' are sought. If the $\overline{K}_{c,min}$ vs C_p^v data for our stationary-bodies are valid for pumping machinery, we can estimate $\overline{K}_{c,min}$ from figure 4.1. This value of $\overline{K}_{c,min}$ may correspond to some finite but currently unknown mean value of ψ'. To use the data on figure 4.1, we must first determine C_p^v for each specific impeller or inducer blade. The latter is a complex task and presents a challenge to the fluid dynamicist; however, a body of information [47-51] exists for these ideal fluid flow calculations. For very small flow incidence angles, values of C_p^v may be estimated from any convenient compilation of air foil data [52,53]. Larger flow incidence angles and/or the requirement for more precise values of C_p^v require the use of computerized numerical solutions to account for the variation in C_p^v with changing ϕ. Once C_p^v is obtained, figure 4.1 can be used to get $K_{c,min}$. Considerable work is required to test the validity of this approach, but it appears that the effort would be justified.

Another simple approach for estimating $\overline{K}_{c,min}$ can be deduced from a rule of thumb suggested by Jakobsen [45]. He suggests that the

conventional[3] cavitation number, K_v, can be estimated from

$$1 + K_v = \left| \overset{v}{C_p} \right| . \qquad (5\text{-}1)$$

To maintain consistency with our predictive formulations, we automatically replace K_v with $\overline{K}_{c,min}$ and there results

$$1 + \overline{K}_{c,min} = \left| \overset{v}{C_p} \right| . \qquad (5\text{-}2)$$

This simple rule of thumb works exceptionally well for the NBS stationary-body data. Using eq (5-2) and the values of $\overset{v}{C_p}$ tabulated on figure 4.1, the reader can readily verify that values of $\overline{K}_{c,min}$ are approximated rather well. It is not at all surprising that eq (5-2) fails to reproduce Billet's data as recorded on figure 4.1. The $\overset{v}{C_p}$ for Billet's zero-caliber ogive data is an experimental value taken from Rouse and McNown [29]. The theoretical value of $\overset{v}{C_p}$ for a zero-caliber ogive is infinite; therefore, any deviation from a true zero-caliber will lower the value of $\overset{v}{C_p}$. Such deviations may result from minute cavity formations or manufacturing imprecisions. Of course, real fluids are also incapable of infinite accelerations around sharp corners. Thus, the true value of $\overset{v}{C_p}$ for zero-caliber ogives may well be higher than 0.64. It may be wiser to use eq (5-2) and the experimental value of $\overline{K}_{c,min}$ from Billet to estimate $\overset{v}{C_p}$ for his blunt-body cylinders. Performing this algebra, we obtain $\overset{v}{C_p} = 1.40$ for

---

[3] K_v and $\overset{v}{C_p}$ may also be written [45] in terms of w_t rather than V_o .

zero-caliber ogives-- a tenable value when extrapolating[4] the $\overset{v}{C}_p$ data of Rouse and McNown [29].

Again, the validity of eq (5-2) should be tested by application to pumping machinery. Once $\overset{v}{C}_p$ is obtained for each value of ϕ, eq (5-2) may supply sufficiently accurate values of $\overline{K}_{c,min}$--again, at a yet to to be determined mean value of ψ'.

5.2 Estimation of $K_{c,min}$ from $\overset{v}{C}_p$ Data (Compilations of experimental $K_{c,min}$ data for similar pumps required)

If the foregoing approaches fail to produce reliable values of $K_{c,min}$ for pumping equipment, it may be necessary to compile $K_{c,min}$ vs ϕ and $\overset{v}{C}_p$ vs ϕ data for various classes (families) of pumps. Such compilations of experimental and theoretical data would permit the development of functional relationships between $K_{c,min}$ and $\overset{v}{C}_p$ for pumping equipment. The following paragraphs outline the type of data needed.

Moore and Meng [6] plotted $K_{c,min}$ vs ϕ for inducers A, B, and C--these data are shown on figure 5.1a. These curves do not reveal any obvious trends with inducer geometry. To account for blade fairing angle, ϕ was normalized and the same data replotted [6]--see figure 5.1b. Still, no geometric trends are apparent. If we replace $K_{c,min}$ with $\left(K_{c,min}\right)_w$, we obtain the results shown on figure 5.2. The original data now resemble a family of curves with definite geometric dependencies. Improvements in the $K_{c,min}$ vs ϕ data for impeller A can also be demonstrated by using $\left(K_{c,min}\right)_w$. This observation merely suggests that $\left(K_{c,min}\right)_w$ may be a good parameter to use in compiling future experimental data. If $\left(K_{c,min}\right)_w$ is used, we should also replace $\overset{v}{C}_p$ with $\left(\overset{v}{C}_p\right)_w$.

---

[4] See p. 25 of reference [29].
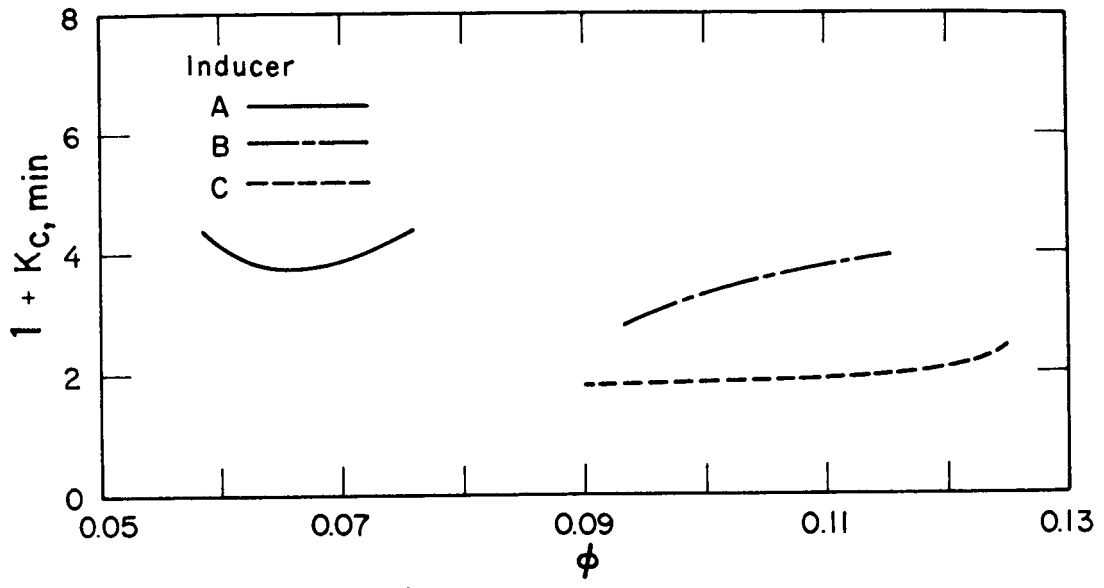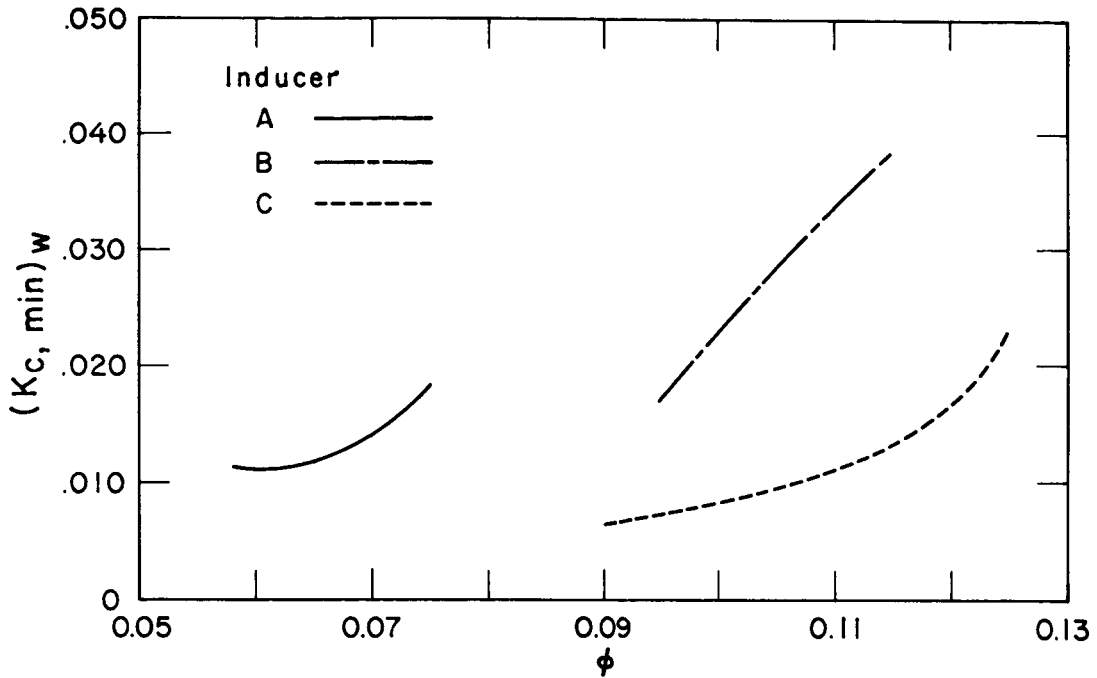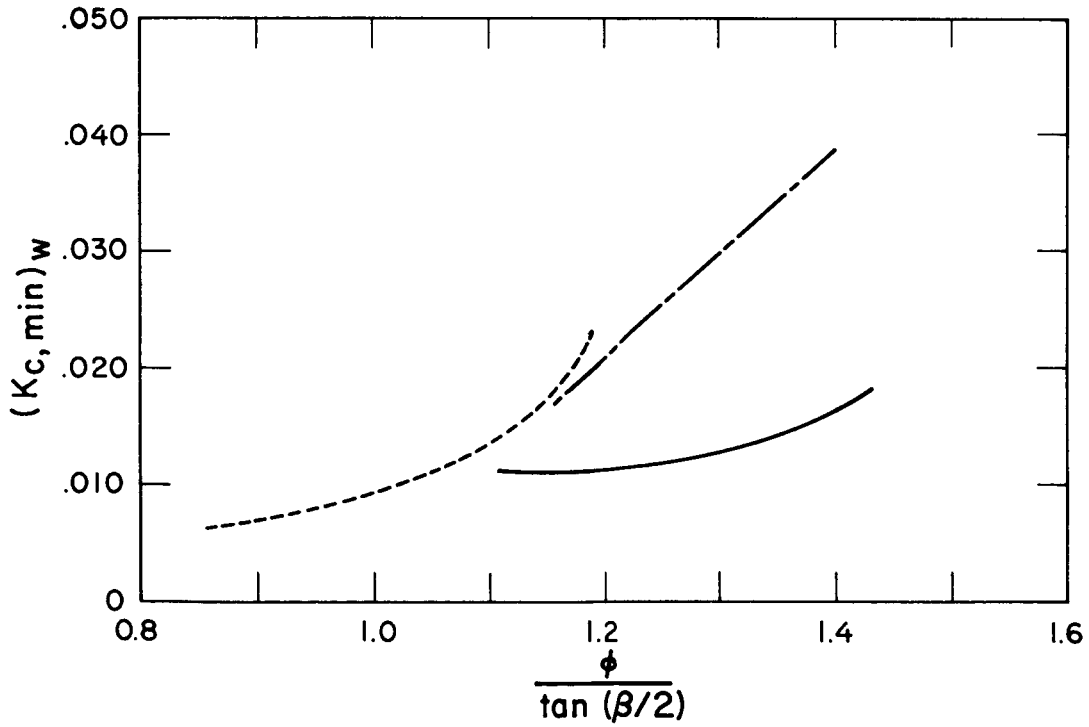
a) Flow Coefficient
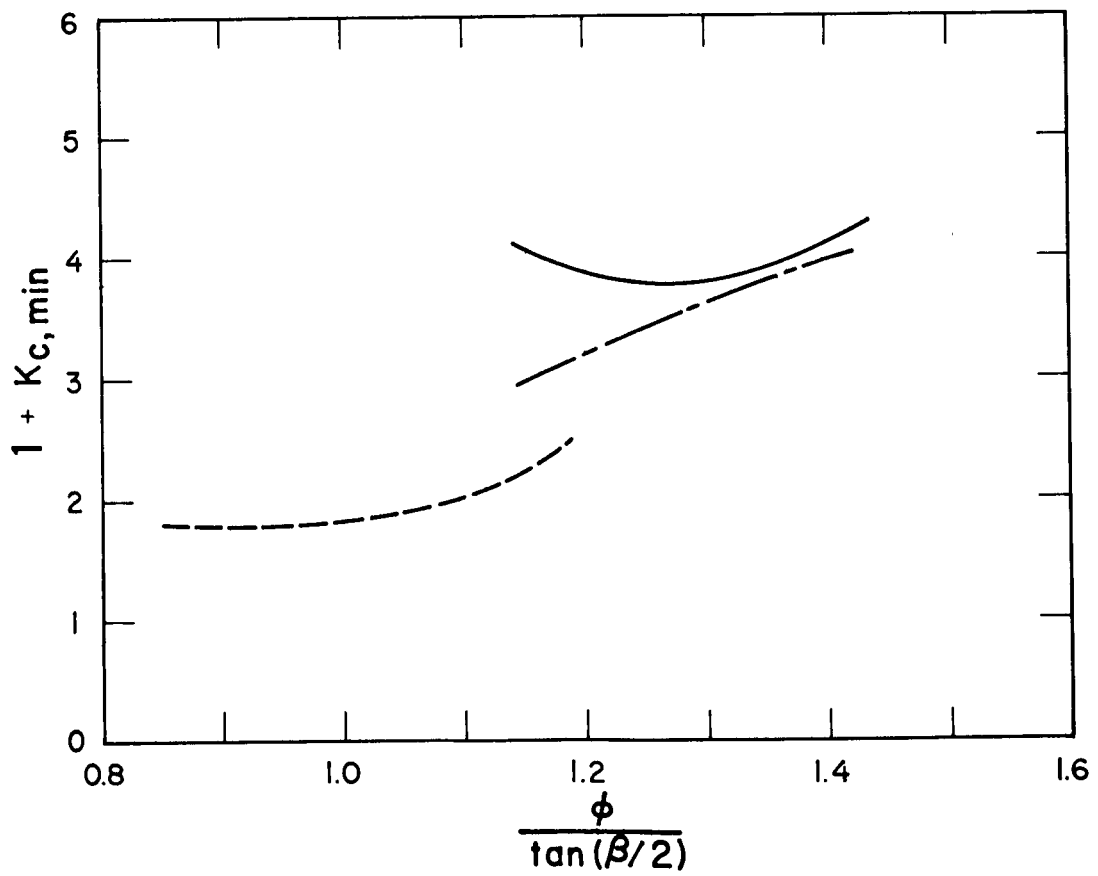
b) Normalized Flow Coefficient

Figure 5.1   Comparison [6] of $K_{c,\,min}$ values for three helical inducers ($\psi' = 0.7$).

56

a) Flow Coefficient

b) Normalized Flow Coefficient

Figure 5.2   Comparison of $(K_{c,\,min})_w$ values for three helical inducers ($\psi' = 0.7$).

Figure 5.3 illustrates a typical inducer blade with the inlet velocity triangle constructed at the blade tip. We shall refer to this figure frequently in that which follows, and $\left(\overset{V}{C_p}\right)_w$ is defined to apply only to the suction surface of the leading edge of the impeller or inducer blade at the tip. $\left(\overset{V}{C_p}\right)_w$ characterizes each specific piece of equipment and is independent of the inlet pressure, temperature, velocity, and the fluid. The $\left(\overset{V}{C_p}\right)_w$ of a hydrodynamic body is constant when the fluid flow is sufficiently turbulent $\left(Re \gtrsim 10^6\right)$ and the flow incidence angle is constant. In pumping equipment Re is normally high, but the angle of flow incidence varies with the flow coefficient ϕ. Thus, the $\left(\overset{V}{C_p}\right)_w$ for a specific piece of equipment may be considered to vary only with ϕ.

$\left(\overset{V}{C_p}\right)_w$ must be invariant if we expect identical cavitation characteristics, so for a prescribed geometry and ψ' it is sufficient to hold ϕ constant. In correlating from one piece of equipment to another, the $\left(C_p\right)_w$ profiles for the two bodies should at least be <u>similar</u>, even though the $\left(C_p\right)_w$ values may be different. The $\left(\overset{V}{C_p}\right)_w$ values may differ because of different tip contour, fairing angle, or cascade solidity at the tip. To obtain similar $\left(C_p\right)_w$ profiles, we must hold θ_1 or θ_2 constant-- either angle may be used depending upon our choice of the blade suction surface or pressure surface as a datum plane.

Because the leading edges of most impellers and inducers are rounded and then faired, we may consider all of them as wedge-shaped bodies with cylindrical noses. While each wedge angle (fairing angle) would produce a different $\left(\overset{V}{C_p}\right)_w$, the $\left(C_p\right)_w$ profiles would be quite similar for the small blade angles under consideration and for constant θ_2. It appears that θ_2 is a most pertinent correlating parameter that accounts for both flow coefficient (ϕ) and blade angle (β). Instead of holding ϕ constant for predictive purposes, we could hold θ_2 constant.

58

Figure 5.3 Nomenclature for typical inducer blade and illustration of inlet tip velocity triangle.

Holding θ_2 constant prescribes specific, but not identical, values of ϕ for each pump. Attempts to correlate the NASA-LeRC pump data holding θ_2 constant were disappointing. Better results were obtained with no restrictions on ϕ as reported in table 4.6.

Referring to figure 5.3, let us consider rotation of a constant velocity vector, w_t, around the blade tip. Note that $w_t \sin \theta_2$ is normal to the pressure surface datum plane and $w_t \cos \theta_2$ is parallel to this datum. Clockwise rotation of w_t: As θ_2 increases the liquid impacts on the suction surface, reducing the peripheral velocity around the leading edge of the blade. This produces higher pressures on the suction surface; therefore, $h_o - \overset{v}{h}$ and $\left(\overset{v}{C_p} \right)_w$ are lowered by clockwise increase in θ_2. Counterclockwise rotation of w_t: As we increase θ_2 in a counterclockwise direction from the pressure surface datum, the liquid must accelerate to flow around the leading edge of the blade. Pressure on the suction surface is lowered causing $h_o - \overset{v}{h}$ and $\left(\overset{v}{C_p} \right)_w$ of the suction surface to increase.

Holding w_t constant and rotating it about the pressure surface datum plane requires a continuous change in ϕ; clockwise rotation of w_t results in larger values of ϕ and counterclockwise rotation produces smaller values of ϕ. The location of the minimum pressure point on the suction surface, and the value of $\left(\overset{v}{C_p} \right)_w$ for the suction surface, will change with each value of ϕ for a particular pump. As ϕ increases-- clockwise increase of θ_2--$\left(\overset{v}{C_p} \right)_w$ decreases, and as ϕ decreases--counter-clockwise increase of θ_2--$\left(\overset{v}{C_p} \right)_w$ increases. Then $\left(\overset{v}{C_p} \right)_w$ is a function of ϕ for any particular piece of equipment.

We can plot calculated $\left(\overset{v}{C_p} \right)_w$ vs ϕ or $\left(\overset{v}{C_p} \right)_w$ vs $\theta_2 / \tan \beta$ and experimental $\left(K_{c,min} \right)_w$ vs ϕ for each pump. We can then determine $\left(K_{c,min} \right)_w$ and $\left(\overset{v}{C_p} \right)_w$ at specific values of ϕ or $\theta_2 / \tan \beta$ for each pump.

The procedure for developing $(K_{c,min})_w$ vs $(\overset{v}{C}_p)_w$ data are illustrated for three helical inducers on figure 5.4. Data similar to those shown in figure 5.4c are required for each value of ψ' of interest. Extensive compilations of such data may make it possible to derive functional relationships between $(K_{c,min})_w$ and $(\overset{v}{C}_p)_w$ for certain classes of pumps. Interpolation or extrapolation of these data to new or different designs may then be possible.

If desired, $(\overset{v}{C}_p)_w$ and $(K_{c,min})_w$ can be expressed in terms of the relative velocity, w_m, for the mean effective blade radius. ϕ changes continuously with radial position along the blade leading edge for constant N, V_o, and β. Under these conditions ϕ is minimum at the blade tip, $(\overset{v}{C}_p)_w$ is a maximum and thus cavitation should originate at the blade tip; therefore, the tip radius was selected as the pump characteristic dimension in this study.
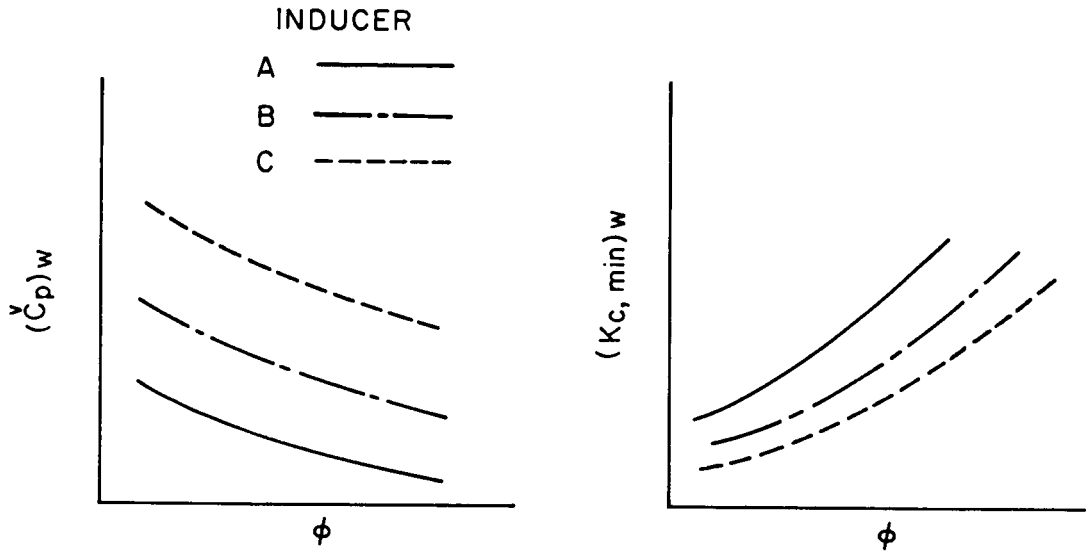
5.3 Estimation of Pump $K_{c,min}$ Using $K_{c,min}$ Data for Stationary-Bodies

(Pump experiments are not required)

This method of estimating $K_{c,min}$ is related to the $\overline{K}_{c,min}$ vs $\overset{v}{C}_p$ approach outlined in subsection 5.1 but is considerably more complex. The following discussion was postponed until now so that the reader could benefit from the foregoing arguments and thus avoid confusion.

On figure 4.1 the NBS stationary-body data are adequately represented by

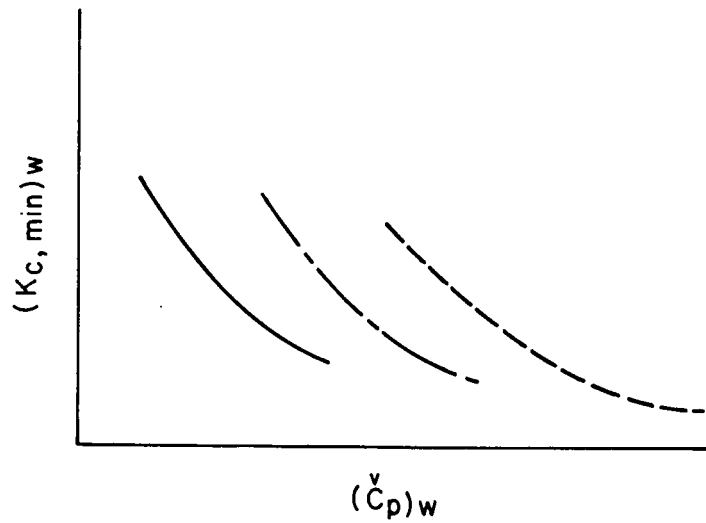$$\left(\overline{K}_{c,min}\right)_{\infty} = 0.30 \overset{v}{C}_p .\qquad (5\text{-}3)$$

Due to the uncertainty in $\overset{v}{C}_p$ for zero-caliber ogives Billet's [28] data were not used in determining the slope of this line. If the Billet

INDUCER
A ———————
B —·—·—·—
C — — — — —

$(\overset{v}{C}_p)_w$

a) Calculated noncavitating $(\overset{v}{C}_p)_w$ (independent of ψ').

$(K_{c,min})_w$

b) Experimental $(K_{c,min})_w$ ($\psi' = $ constant).

$(K_{c,min})_w$

$(\overset{v}{C}_p)_w$

c) Experimental $(K_{c,min})_w$ and calculated $(\overset{v}{C}_p)_w$ ($\psi' = $ constant).

Figure 5.4   Development of $(K_{c,min})_w$ vs $\left(\overset{v}{C}_p\right)_w$ data for a family of helical inducers ($\psi' = $ constant).

data are forced to fit this straight line, we obtain $\overset{v}{C}_p = 1.26$ and $\left(\overset{v}{C}_p\right)_\infty = 1.20$ for his zero-caliber ogives. Using the area correction factor, F_C, eq (5-3) can be replaced by the equivalent expression

$$F_C^2 \, \overline{K}_{c,\min} \approx 0.30 \left(\overset{v}{C}_p\right)_\infty . \qquad (5-4)$$

Equation (5-4) assumes that F_C is about the same for cavitating and noncavitating flows. This is a fair approximation for the relatively thin cavities developed on the stationary-bodies and for average cavity lengths associated with $\overline{K}_{c,\min}$. In pump blade passages, the cavity thickness is frequently many times the blade thickness; therefore, the cavity shape can dominate F_C for cavitating pumps. Accordingly, F_C must account for the presence of cavities when applied to pumps.

In deriving the data represented by eq (5-4) it was noticed that $F_C^2 \, \overline{K}_{c,\min} \approx$ constant for all of the stationary-body data. Because $\overline{K}_{c,\min}$ from Billet is not in doubt, his data were included with the NBS data to obtain

$$F_C^2 \, \overline{K}_{c,\min} \approx 0.374 . \qquad (5-5)$$

An expression of this variety has great appeal because F_C inherently accounts for some of the detailed blade-plus-cavity geometry of each individual pump. This appeal exists even though the constant in eq (5-5) may be expected to vary for different classes of pumps and for different values of ψ'. Assuming the applicability of this expression to pumps, we seek means of computing F_C for cavitating equipment. To simplify this computation, we will use the basic cascade configuration illustrated in figure 5.5. This simple configuration is adequate for the inducers correlated herein but will require some modifying assumptions for application to the impellers.
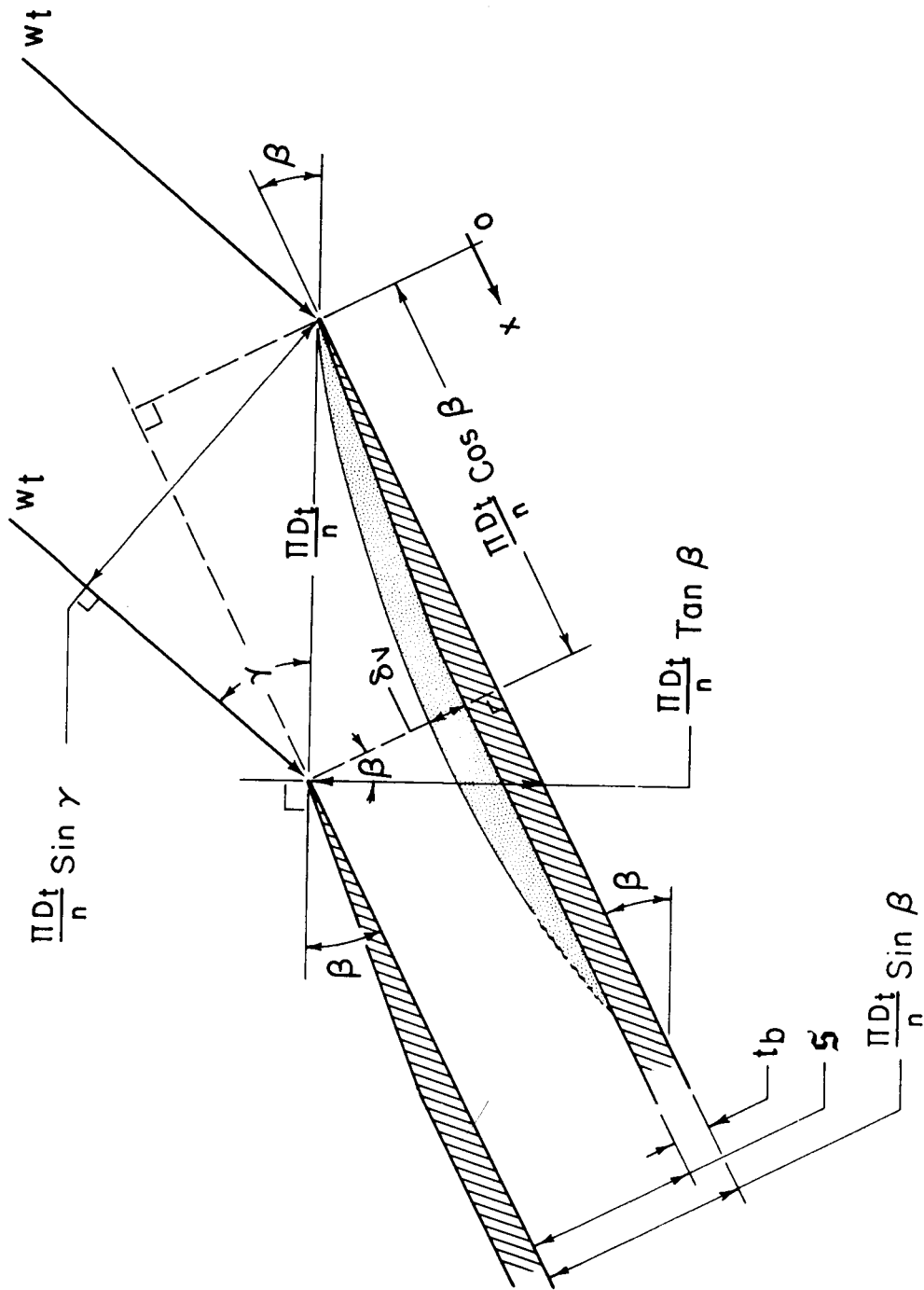
63

Figure 5.5   Cascade configuration illustrated for computation of F_C in cavitating inducers and impellers.

To evaluate F_C, we must determine the blocked and unblocked areas of the blade passages as they appear to an observer traveling with a particle of fluid along the velocity vector w_t. The unblocked area is taken as

$$\left(\frac{\pi D_t \, \text{Sin} \, \gamma}{n}\right) \left(\frac{D_t - D_h}{2}\right) \qquad (5\text{-}6a)$$

and the blocked area is described by

$$\left(s - \delta_v\right)\left(\frac{D_t - D_h}{2}\right) , \qquad (5\text{-}6b)$$

where $s = \left(\frac{\pi D_t}{n} \, \text{Sin} \, \beta - t_b\right)$.

By definition

$$F_C = \left(\frac{s - \delta_v}{\frac{\pi D_t \, \text{Sin} \, \gamma}{n}}\right)^2 . \qquad (5\text{-}7)$$

To evaluate δ_v we use the expression for cavity shapes derived from our ogive studies (see discussion in section 4.3.3 of this report),

$$\delta_v = 0.41 \, x^{0.75} . \qquad (5\text{-}8a)$$

Converting δ_v and x in eq (5-8a) from millimeters to centimeters, we obtain

$$\delta_v = 0.231 \, x^{0.75} , \qquad (5\text{-}8b)$$

where x cannot exceed $\ell/2$.

Equation (5-8b) must be adjusted to account for the effect of the modified cascade solidity on cavity thickness. In our preliminary hydrofoil and ogive tests we observed that cavity thickness decreased almost linearly with increasing solidity (blockage) as it is normally defined in turbomachinery design. To adapt eq (5-8b) to the pump data, we note

65

that the noncavitating blockage factor, F_B, for the stationary-bodies is analogous to t_b/s for the pumps. F_B for the quarter-caliber ogives was 0.095, nearly the same value as t_b/s for impeller B (see table 5.1). Thus, we will assume that eq (5-8b) is applicable to the prediction of cavity shapes within the blades of impeller B and will linearly correct this equation for solidity effects in the other equipment. The most meaningful noncavitating solidity parameter at our disposal is the modified cascade solidity at the tip, C_{st}. From table 4.4 we obtain $C_{st} = 1.683$ for impeller B and then eq (5-8b) may be rewritten in the generalized form

$$\delta_v = 0.231 \left(\frac{1.683}{C_{st}}\right) (x)^{0.75} . \tag{5-9}$$

Equations (5-7) and (5-9) may now be used to evaluate F_C for all of the NASA-LeRC pumps. Any reasonable value of x may be inserted into eq (5-9)--the unblocked blade chord length, C_{ub}, was used herein. All of the geometry and flow parameters necessary to evaluate these two expressions are contained in tables 4.4 and 5.1. Most of the geometry data given in tables 4.4 and 5.1 are readily calculable according to the illustration given in figure 5.5; however, some of the impeller data required measurement of the equipment and/or reference to construction drawings.

In table 5.1, the values of s for the impellers are not the true measured values but are calculated as shown on figure 5.5 and in the footnote of table 5.1. The calculated values were used after careful study of a NASA cavitation film [30]. This film, for a pump similar to impeller B, revealed that vapor always fills the space adjacent to the suction surface of the impeller blades (see figure 5.6). From this observation and for simplicity of analysis, we are effectively straightening the impeller vanes to conform to the illustration in figure 5.5. For these impellers

Table 5.1 Estimation of $\overline{K}_{c,min}$ From $F_C^2 \overline{K}_{c,min} = 0.374$.

Pump	φ	β	γ	Sin β	Sin γ	$\frac{\pi D_t}{n}$ (cm)	s* (cm)	t_b/s	δ_v (cm)	F_C	Predicted[1] $\overline{K}_{c,min}$ (ψ' = ?)	Experimental[2] $\overline{K}_{c,min}$ (ψ' = 0.7)	$F_C^2 (\overline{K}_{c,min})_E$ (ψ' = 0.7)
Impeller A	0.225	18.7°	12.683°	0.3206	0.2196	1.775	0.3691	0.542	0.1195	0.4100	2.22	1.40	0.2357
	.245	"	13.767	"	.2380	"	"	"	"	.3490	3.07	1.16	.1417
	.260	"	14.567	"	.2515	"	"	"	"	.3126	3.83	---	---
Impeller B	0.440	22.°	23.750°	0.3746	0.4027	4.398	1.490	0.106	0.5874	0.2597	5.54	5.48	0.3694
Inducer A	0.060	6.°	3.433°	0.1045	0.0599	13.262	1.216	0.140	0.7258	0.3808	2.58	---	---
	.065	"	3.717	"	.0648	"	"	"	"	.3253	3.53	3.06	0.3238
	.070	"	4.000	"	.0698	"	"	"	"	.2804	4.76	3.09	.2430
	.075	"	4.283	"	.0747	"	"	"	"	.2448	6.24	3.42	.2050
Inducer B	0.100	9.4°	5.717°	0.1633	0.0996	13.246	1.909	0.133	1.1150	0.3622	2.85	---	---
	.105	"	6.000	"	.1045	"	"	"	"	.3290	3.46	2.74	0.2965
	.110	"	6.283	"	.1094	"	"	"	"	.3002	4.15	3.02	.2722
	.115	"	6.567	"	.1144	"	"	"	"	.2745	4.96	3.18	.2396

* Calculated from $s = (\pi D_t/n) \sin \beta - t_b$; Actual spacing is larger than calculated s for impeller A and B due to curvature of impeller vanes, see figure 5.6.

1 Predicted from $\overline{K}_{c,min} = 0.374/F_C^2$.

2 Calculated from experimental data $\left[\equiv (\overline{K}_{c,min})_E \right]$.
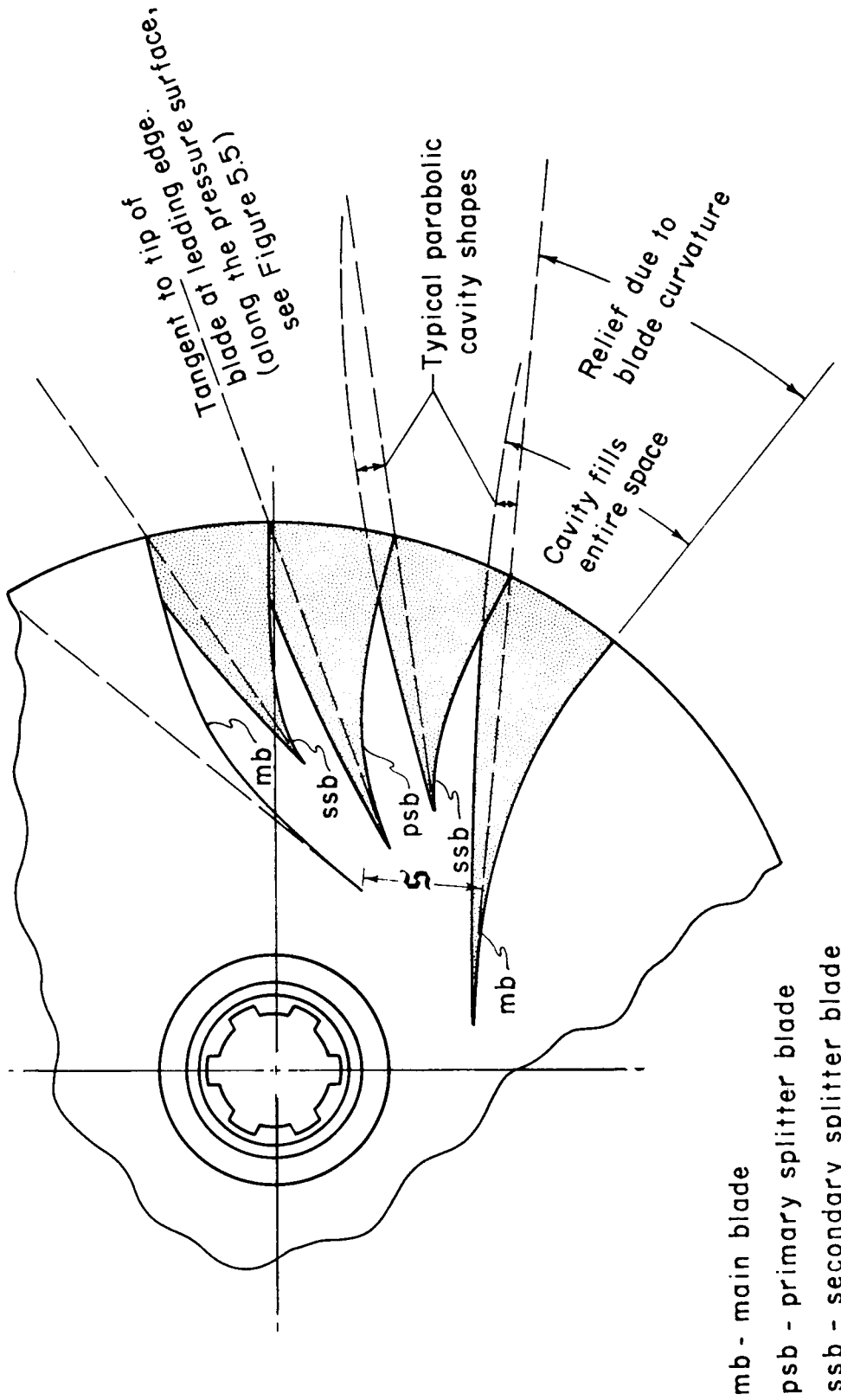
Figure 5.6 Developed cavitation on impeller vanes.

mb – main blade
psb – primary splitter blade
ssb – secondary splitter blade

the cavity is assumed to have the additional thickness--measured from the theoretical straightened vane position--as specified by eq (5-9). Again, this concept is illustrated in figure 5.6.

Equations (5-5), (5-7), and (5-9) were applied to the NASA-LeRC impeller and inducer data and the results are presented in table 5.1. The predicted values of $\overline{K}_{c,min}$ are remarkably close to the experimental values obtained from our previous calculations. These predicted values of $\overline{K}_{c,min}$ do not correspond to known values of ψ' as explained in the following paragraph. For simplicity, inlet blade tip dimensions were used to evaluate the geometry parameters in this two-dimensional cascade flow illustration. In reality, the flow is much more complex (particularly for the impellers) and could be treated to account for variation in blade height, curvature, thickness, etc. Also, mean effective dimensions might be formulated to produce better results in the simplified analysis. Only a modest effort was expended in this direction because so many possibilities exist; arithmetic mean values of blade thickness, modified cascade solidity, $\mathfrak{s}$, etc., were tried and they produced much higher values of $\overline{K}_{c,min}$ than those listed in table 5.1. Perhaps the initial choice of inlet blade tip dimensions was fortuitous because it is apparent that prediction of $\overline{K}_{c,min}$ from eq (5-5) is highly sensitive to choice of physical dimensions. More detailed analysis is needed to improve $\overline{K}_{c,min}$ predictions by this method.

Possibly the major deficiency of this approach is that we have no idea what value of ψ' corresponds to our predicted $\overline{K}_{c,min}$; i.e., we must determine what head loss is attributable to a cavity of half-length C_{ub}. Obviously this head loss, and therefore ψ', will vary with each pump. Theoretically, $\overline{K}_{c,min} \rightarrow \left| C_p^v \right|$ as $\psi' \rightarrow 1.0$. Also, $S_c \rightarrow S_{nc}$ as $\psi' \rightarrow 1.0$. To pursue this idea, we must establish

69

relationships between $\overline{K}_{c,min}$ and ψ' for each specific pump. At least two potential methods exist for accomplishing this task--both are described below.

This blade-plus-cavity approach may be salvaged by performing idealized flow calculations to evaluate the cavitating head loss. These computations are performed at constant N and Q for a pump of known geometry. Cavity shape is predicted by eq (5-9) for an assumed cavity length and a corresponding value of $\overline{K}_{c,min}$ is calculated. Head loss is then computed by assuming that the cavity behaves like a solid body, i.e., by assuming that the blades have the shape of blade-plus-cavity. This head loss is converted to ψ' for identification with its companion $\overline{K}_{c,min}$. Such computations are not simple, but even rough estimates should be adequate to establish the needed relationship between predicted $\overline{K}_{c,min}$ and ψ'. Computerized solutions based on incremented cavity lengths may be terminated when the desired ψ' is reached. The corresponding cavity length is then used to evaluate $\overline{K}_{c,min}$ as previously described. Next, $\overline{K}_{c,min}$ is used to evaluate pump NPSH requirements using eqs (4-16) and the method described herein.

More experimental pump data and analytical work are required to confirm or invalidate this approach.

A second method of linking $\overline{K}_{c,min}$ and ψ' requires experimentally verified $\mathcal{V}_v$ vs ψ' data. Knowing the pump geometry and using eqs (5-9), (5-7), and (5-5), we can calculate δ_v, F_C, $\overline{K}_{c,min}$ and $\mathcal{V}_v$ for each assumed value of x; therefore, functional relationships between $\overline{K}_{c,min}$ and $\mathcal{V}_v$ may be derived for each pump. By relating $\mathcal{V}_v$ to ψ', we can establish the needed $\overline{K}_{c,min}$ vs ψ' data. Experimental data, with intra-blade flow visualization, is required to establish the $\mathcal{V}_v$ vs ψ' function for each class of pumps. Thus, this method of evaluating ψ' has no appeal unless a simple and universal correlation between $\mathcal{V}_v$ and ψ' is discovered.

In eq (4-21) we reasoned that $\mathcal{V}_v \propto (1-\psi')$. We unsuccessfully attempted to relate $K_{c,min}$ to $\mathcal{V}_v$ in our stationary-body tests. $K_{c,min}$ was found to be independent of $\mathcal{V}_v$ for the venturi and hydrofoil and was weakly related for the ogives ($K_{c,min} \propto \mathcal{V}_v^{-0.05}$). From Billet's data [28], it was deduced that $K_{c,min} \propto \mathcal{V}_v^{-0.16}$. Substituting $C_1 (1-\psi')$ for $\mathcal{V}_v$, we may write

$$K_{c,min} = C_1' \left(\frac{1}{1-\psi'}\right)^z , \qquad (5\text{-}10a)$$

or

$$\frac{K_{c,min}}{(K_{c,min})_{ref}} = \left(\frac{(1-\psi')_{ref}}{1-\psi'}\right)^z , \qquad (5\text{-}10b)$$

where the body or pump geometry is held constant. To test this simple expression, values of z were computed for the impellers and inducers. These values were just as inconsistent as those for the stationary-bodies. Thus, the assumption that $K_{c,min} \propto \mathcal{V}_v^{-z}$ fails and eq (5-10b) cannot be used to transfer $K_{c,min}$ data from one ψ' to another.

The prospects of acquiring experimental verification of universal functions that relate $\mathcal{V}_v$ and ψ' are currently dim. Nevertheless, this method of coupling ψ' and $\overline{K}_{c,min}$ is sufficiently obvious to justify the effort expended herein.

6. SUGGESTIONS FOR FUTURE WORK AND DATA COMPILATIONS

This study has revealed a number of areas where future work is needed. Each of the tasks listed below will require considerable effort from the scientific community and pumping machinery specialists.

1) Improve the accuracy and consistency of fluid thermophysical properties--particularly for conventional fluids such as water, hydrocarbons, and the common refrigerants.

2) Launch a significant effort to collect existing pump data (unpublished and published), together with geometric details of pumps, for purposes of correlation and to test correlative-predictive procedures outlined in this report.

3) Provide the type of data indicated in this report and provide the maximum in geometric detail for all future pump experimentation. Expend maximum effort to obtain data of the highest possible quality and precision.

4) Evaluate the potential methods of estimating $K_{c,min}$ outlined herein and establish C_p^v - $K_{c,min}$ - ϕ relationships with pump data compilations.

5) Improve and simplify, if possible, C_p^v calculations.

6) Perform additional stationary-body work because this study and previous work [3] show the relevance of such work and its direct applicability to the prediction of cavitating performance in rotating machinery.

7) Finally, as a result of additional knowledge and experience, improve the existing correlative expressions.

7. CONCLUDING REMARKS

The work performed in the course of this study is documented in the four volumes of this report series and may be succinctly summarized as follows:

1) A simplified, more precise computation [23] was devised for the calculation of B-factors. This improved method is based upon isentropic vaporization of liquid and clearly demonstrates that precise thermophysical properties of fluids are required for improved future work.

2) Convective heat transfer and two-phase mass flux limiting concepts were used [21] to extend and improve existing formulae for correlating developed cavitation data. These correlative expressions were extended to the prediction of cavitating performance of pumps in this final volume (IV).

3) Extensive developed-cavity data were acquired for three different hydrodynamic body shapes using liquid hydrogen and liquid nitrogen test fluids. These data were obtained using two-dimensional and axisymmetric bodies and for both internal [20] and external flows. Size effects were obtained for the submerged axisymmetric bodies [22].

4) The results of work performed in items (1) and (2) were used to correlate the data obtained in item (3).

5) The liquid hydrogen pump data generated by NASA-LeRC were analyzed and correlated using the results obtained from items (1), (2), (3), and (4). Thus, the state-of-the-art of predicting cavitating performance of pumping equipment was significantly extended.

6) The relevance (to pumps) of analysis and experimentation with stationary bodies was strengthened; i.e., the correlative expressions derived for stationary bodies appear extendible to rotating equipment.

7) The effort expended in items (1) through (6) revealed certain technical areas where additional analysis and experimentation are needed--these areas are defined.

8. NOMENCLATURE

a_ℓ = adiabatic acoustic velocity of liquid, evaluated at the minimum cavity pressure

a_v = adiabatic acoustic velocity of vapor, evaluated at the minimum cavity pressure

A_o = inlet area of test section (tunnel); may also be inlet area in line-mounted pump impellers or pump inducers

B = ratio of vapor to liquid volume associated with the sustenance of a fixed cavity in a liquid $[\equiv \mathcal{V}_v / \mathcal{V}_\ell]$

$BFLASH$ = B derived from isentropic flashing theory (Ref. [23])

B_t $\equiv$ BFLASH

C_h = chord length of inlet blade at hub, see table 4.4

C_n = (n = 0, 1 . . . etc.): constants or numerical coefficients in various algebraic expressions

C_p = noncavitating pressure coefficient $[\equiv (h_x - h_o)/(V_o^2/2g_c)]$

$\overset{v}{C}_p$ = minimum noncavitating pressure coefficient $[\equiv (\overset{v}{h} - h_o)/(V_o^2/2g_c)]$

$(\overset{v}{C}_p)_w$ = minimum noncavitating pressure coefficient based on inlet blade tip relative velocity $[\equiv (\overset{v}{h} - h_o)/(w_t^2/2g_c) = \overset{v}{C}_p \phi^2/(1 + \phi^2)]$

$\left(\overset{v}{C}_p\right)_\infty$ = value of $\overset{v}{C}_p$ in an infinite flow field $\left[\equiv F_C(\overset{v}{C}_p)\right]$

$C_{p,\ell}$ = specific heat of liquid at constant pressure, evaluated at the tunnel (pump) inlet (P_o and T_o)

C_{st} = modified cascade solidity at tip of inlet blade $\left[\equiv C_t/C_{ub}\right]$; note that this solidity parameter is equivalent to the conventional definition of cascade solidity divided by $\cos\beta$

C_t = chord length of inlet blade at tip, see table 4.4

C_{ub} = unblocked chord length of inlet blade at tip, see table 4.4

D = characteristic dimension of stationary-body or pump equipment; taken as radius of contour for stationary-bodies and as inlet blade tip diameter for impellers and inducers

D_D = discharge (overall) diameter of impeller

D_h = hub diameter of inlet blade at the inlet

$D_{h,ps}$ = hub diameter of primary splitter vanes on impellers

$D_{h,ss}$ = hub diameter of secondary splitter vanes on impellers

D_{m1} = inlet blade mean effective diameter for impellers or inducers $\left[\equiv\sqrt{\dfrac{D_t^2 + D_h^2}{2}}\right]$

D_{m2} = impeller mean effective diameter $\left[\equiv\sqrt{\dfrac{n D_t^2 + n D_{t,ps}^2 + 2n D_{t,ss}^2}{4n}}\right]$

D_{m3} = impeller mean effective diameter $\left[\equiv\sqrt{\dfrac{n D_{m1}^2 + n D_{m,ps}^2 + 2n D_{m,ss}^2}{4n}}\right]$

76

$D_{m,ps}$ = mean effective diameter of primary splitter vanes $\left[\equiv \sqrt{\dfrac{D_{t,ps}^2 + D_{h,ps}^2}{2}}\right]$

$D_{m,ss}$ = mean effective diameter of secondary splitter vanes $\left[\equiv \sqrt{\dfrac{D_{t,ss}^2 + D_{h,ss}^2}{2}}\right]$

D_o = tunnel inlet diameter for stationary-bodies or inlet duct diameter for impellers and inducers

D_t = tip diameter of inlet blade at the inlet

$D_{t,ps}$ = inlet tip diameter of primary splitter vanes on impellers

$D_{t,ss}$ = inlet tip diameter of secondary splitter vanes on impellers

F_B = area blockage factor, the fraction of cross sectional flow area occupied by the stationary-body or by the pump blade-plus-cavity

F_C = area correction factor, the square of the ratio of blocked cross sectional flow area to unblocked (inlet) cross sectional flow area $\left[\equiv \left(1 - F_B\right)^2\right]$

Fr = Froude number $\left[\equiv V_o/\sqrt{\ell}\,\right]$

g_c = conversion factor in Newton's law of motion (gravitational acceleration)

$h_{c,min}$ = minimum static head in cavitated region corresponding to minimum absolute static pressure within the cavity

h_o = tunnel or pump inlet static head corresponding to absolute static inlet pressure

h_v = head corresponding to saturation (or vapor) pressure of the test liquid at the tunnel (pump) inlet temperature, T_o

h_x = static head corresponding to absolute static pressure, measured on the stationary-body or on the suction surface of the pump inlet blade at distance x, downstream of the minimum pressure point--for non-cavitating flow

$\overset{v}{h}$ = static head corresponding to the minimum absolute static pressure on the leading edge of the stationary-body or on the suction surface of the pump inlet blade, computed from expression for $\overset{v}{C}_p$

Δh_v = static head depression attributable to the vaporization of liquid that is required to sustain a developed cavity $\left[\equiv h_v - h_{c,min} \right]$

H = total head, corresponds to total pressure

ΔH_c = total head rise across cavitating pump impeller or inducer

ΔH_{nc} = total head rise across noncavitating pump impeller or inducer

k = thermal conductivity of liquid, evaluated at tunnel inlet or at pump inlet (P_o and T_o)

$K_{c,min}$ = developed cavitation parameter, based on minimum static cavity pressure $\left[\equiv \left(h_o - h_{c,min} \right) / \left(V_o^2 / 2g_c \right) \right]$

$\overline{K}_{c,min}$ = arithmetic mean value of $K_{c,min}$ for a complete set of data points for a particular hydrodynamic body-fluid combination or for a particular pump at mean values of ψ'; also used for arithmetic mean value of $K_{c,min}$ at specific operating conditions for a particular pump

78

$\left(\overline{K}_{c,min}\right)_\infty$ = value of $\overline{K}_{c,min}$ in an infinite flow field $\left[\equiv F_C\left(\overline{K}_{c,min}\right)\right]$

$\left(K_{c,min}\right)_w$ = developed cavitation parameter, based on inlet blade tip relative velocity $\left[\equiv\left(h_o - h_{c,min}\right)/\left(w_t^2/2g_c\right) = K_{c,min}\phi^2/\left(1+\phi^2\right)\right]$

K_v = conventional developed cavitation parameter $\left[\equiv\left(h_o - h_v\right)/\left(V_o^2/2g_c\right)\right]$

ℓ = length of cavities developed on stationary-bodies or on pump blades, used interchangeably with x

MPE = arithmetic mean percent error in predicted values of NPSH--see tables 4.5 through 4.7

MTWO = liquid phase velocity ratio $\left[\equiv V_o/V_\ell = \dfrac{V_o}{a_\ell}\left\{\dfrac{1 + B\left(\rho_\ell/\rho_v\right)\left(a_\ell/a_v\right)^2}{1 + B\left(\rho_v/\rho_\ell\right)}\right\}^{0.5}\right]$, see reference [21]

n = number of inlet (main) blades on impeller or inducer

n_{ps} = number of primary splitter vanes on impeller

n_{ss} = number of secondary splitter vanes on impeller

N = angular velocity of pump impeller or inducer

NPSH = net positive suction head $\left[\equiv h_o + \left(V_o^2/2g_c\right) - h_v\right]$

Pe = Peclet number $\left[\equiv V_o\ell/\alpha\right]$

PE = peripheral extent of blades, degrees of arc

P_o = tunnel or pump absolute static inlet pressure

Pr	=	Prandtl number $\left[\equiv C_{p,\ell}\mu/k \right]$
Q	=	volumetric flow rate (capacity) of pump
Re_D	=	diameter Reynolds number $\left[\equiv \rho_o V_o D/\mu \right]$
Re_ℓ	=	length Reynolds number $\left[\rho_o V_o \ell/\mu \right]$
Δ	=	peripheral length along the contour of a stationary-body as measured from the leading edge of the contour to the minimum pressure point on the contour
s_{f1}	=	specific entropy of saturated liquid at T_o
s_{f2}	=	specific entropy of saturated liquid at minimum cavity pressure (temperature)
s_{v2}	=	specific entropy of saturated vapor at minimum cavity pressure (temperature)
S_{nc}	=	noncavitating suction specific speed of pump
S_c	=	cavitating suction specific speed of pump
s	=	the minimum distance (with allowance for blade thickness) between impeller or inducer blades as measured between lines constructed tangent to the blade pressure surfaces at the blade tips, see figures 5.5 and 5.6 $\left[\equiv (\pi D_t/n) \sin \beta - t_b \right]$
t_b	=	thickness of all blades on the impellers: tip thickness for inducer blades
T_o	=	bulkstream static temperature of liquid entering the tunnel or pump
u_t	=	pump inlet blade tip speed

V_ℓ = characteristic liquid velocity component, normal to cavity liquid-vapor interface, see reference [21]

V_o = bulkstream velocity of test liquid at inlet to tunnel or pump

VHO = experimental developed cavity data for the combined venturi, hydrofoil, and ogive stationary-bodies

$\tilde{V}_\ell$ = volume of liquid associated with the sustenance of a developed cavity

$\tilde{V}_v$ = volume of vapor associated with the sustenance of a developed cavity

We_ℓ = Weber number $\left[\equiv \rho_o V_o^2 \ell/\sigma \right]$

w_t = liquid velocity relative to pump inlet blade at tip $\left[\equiv \sqrt{V_o^2 + u_t^2} \right]$

x = axial distance measured from minimum pressure point on stationary-bodies; also used to measure cavity length along impeller and inducer blade chords

Greek

α = thermal diffusivity of liquid, evaluated at tunnel (pump) inlet (P_o and T_o)

β = inlet (main) blade angle at tip--measured from circumferential direction, see table 4.4 and figure 5.3

β_1 = blade leading edge fairing angle $[\equiv \beta/2]$

γ = $\tan^{-1}\phi$

81

δ_v　　＝　　thickness of the developed vaporous cavity

θ_1　　＝　　angle between blade suction surface and w_t

θ_2　　＝　　angle between blade pressure surface and w_t

μ　　＝　　absolute viscosity of liquid, evaluated at tunnel (pump) inlet (P_o and T_o)

ν　　＝　　kinematic viscosity of liquid, evaluated at tunnel (pump) inlet [$\equiv \mu/\rho_o$]

ρ_ℓ　　＝　　density of liquid, evaluated at minimum cavity pressure

ρ_o　　＝　　density of liquid, evaluated at tunnel (pump) inlet (P_o and T_o)

ρ_v　　＝　　density of vapor, evaluated at minimum cavity pressure

σ　　＝　　surface tension of liquid in contact with its vapor, evaluated at tunnel (pump) inlet (P_o and T_o)

ϕ　　＝　　flow coefficient [$\equiv V_o/u_t$]

ψ　　＝　　head rise coefficient [$\equiv g_c \Delta H/u_t^2$]

ψ'　　＝　　ratio of cavitating to noncavitating head rise coefficients [$\equiv \Delta H_c/\Delta H_{nc}$]

Subscripts

o　　＝　　denotes tunnel (pump) inlet location

ref　　＝　　reference run (data point), or test conditions, to which a computation is being referenced when attempting to correlate pump cavitation performance via eqs(4-14) or eqs(4-16) and when using eq (4-1) or eq (4-2)

82

Superscripts

E1   =   exponent on thermal diffusivity ratio in eq (4-1) and eq (4-2)

E2   =   exponent on tunnel inlet velocity ratio in eq (4-1) and also used as an exponent on the MTWO ratio in eq (4-2)

E3   =   exponent on cavity length ratio in eq (4-1) and eq (4-2)

E4   =   exponent on kinematic viscosity ratio in eq (4-1) and eq (4-2)

E5   =   exponent on surface tension ratio in eq (4-1) and eq (4-2)

E6   =   exponent on characteristic dimension ratio in eq (4-1) and eq (4-2)

p   =   exponent in algebraic expression for cavity shape ($\delta_v = C_o x^p$)

z   =   exponent in algebraic expression, defined by eqs (5-10)

9. REFERENCES

1. Pinkel, I., Hartmann, M. J., Hauser, C. H., Miller, M. J.,
   Ruggeri, R. S., and Soltis, R. F., Pump technology, Chap.
   VI, pp. 81-101, taken from Conference on Selected Technology
   for the Petroleum Industry, NASA SP-5053 (1966).

2. Erosion by Cavitation or Impingement, STP-408, 288 pages
   (1967), available from ASTM, 1916 Race Street, Philadelphia,
   Pa., 19103.

3. Moore, R. D., and Ruggeri, R. S., Prediction of thermodynamic
   effects of developed cavitation based on liquid hydrogen and
   freon-114 data in scaled venturis, NASA Tech. Note D-4899
   (Nov. 1968).

4. Ruggeri, R. S., and Moore, R. D., Method for prediction of
   pump cavitation performance for various liquids, liquid tem-
   peratures, and rotative speeds, NASA Tech. Note D-5292
   (June 1969).

5. Moore, R. D., Prediction of pump cavitation performance,
   Proc. Int. Symp. on the Fluid Mechanics and Design of
   Turbomachinery, Pennsylvania State Univ., University Park,
   Pa., Aug. 30 - Sept. 3, 1970, NASA - SP 304.

6. Moore, R. D., and Meng, P. R., Comparison of noncavitation
   and cavitation performance for 78°, 80.6°, and 84° helical
   inducers operated in hydrogen, NASA Tech. Note D-6361
   (May 1971).

7. Spraker, W. A., Two-phase compressibility effects on pump
   cavitation, Symposium on Cavitation in Fluid Machinery,
   presented at winter meeting, Chicago, Ill., Nov. 7-11, 1965,
   pp. 162-171 (ASME, New York, N.Y.).

8. Jakobsen, J. K., On the mechanism of head breakdown in cavitating inducers, Trans. ASME, Ser. D, 86, No. 2, 291-305 (June 1964).

9. Chivers, T. C., Cavitation in centrifugal pumps, first and second papers, Proc. Inst. Mech. Engrs. 184, Part 1, No. 2, 37-68 (1969-70).

10. Fisher, R. C., Discussion of "A survey of modern centrifugal pump practice for oilfield and oil refining services" by N. Tetlow, Proc. Inst. Mech. Engrs. 152, 305-306 (Jan. - Dec. 1945).

11. Stahl, H. A., and Stepanoff, A. J., Thermodynamic aspects of cavitation in centrifugal pumps, Trans. ASME 78, No. 8, 1691-1693 (Nov. 1956).

12. Jacobs, R. B., Prediction of symptoms of cavitation, J. Res. Nat. Bur. Stand. (U.S.), 65C (Eng. and Instr.), No. 3, 147-156 (July - Sept. 1961).

13. Hollander, A., Thermodynamic aspects of cavitation in centrifugal pumps, ARS J. 32, 1594-1595 (Oct. 1962).

14. Stepanoff, A. J., Centrifugal and Axial Flow Pumps, pp. 256-265 (John Wiley and Sons, Inc., New York, N.Y., 1957).

15. Stepanoff, A. J., Cavitation properties of liquids, ASME J. of Engr. for Power 86, No. 2, 195-200 (Apr. 1964).

16. Saleman, Victor, Cavitation and NPSH requirements of various liquids, ASME J. of Basic Engr. 81, No. 2, 167-180 (June 1959).

17. Wilcox, W. W., Meng, P. R., and Davis, R. L., Performance of an inducer-impeller combination at or near boiling conditions for liquid hydrogen, Book, Advances in Cryogenic Engineering 8, Ed. K. D. Timmerhaus, pp. 446-455 (Plenum Press, Inc., New York, N. Y., 1963).

18. Spraker, W. A., The effects of fluid properties on cavitation in centrifugal pumps, ASME J. of Engr. for Power $\underline{87}$, No. 3, 309-318 (July 1965).

19. Gelder, T. F., Ruggeri, R. S., and Moore, R. D., Cavitation similarity considerations based on measured pressure and temperature depressions in cavitated regions of freon-114, NASA Tech. Note D-3509 (July 1966).

20. Hord, J., Anderson, L. M., and Hall, W. J., Cavitation in liquid cryogens, Volume I: Venturi, NASA Rept. CR-2054 (May 1972).

21. Hord, J., Cavitation in liquid cryogens, Volume II: Hydrofoil, NASA Rept. CR-2156 (Jan. 1973).

22. Hord, J., Cavitation in liquid cryogens, Volume III: Ogives, NASA Rept. CR-2242 (May 1973).

23. Hord, J., and Voth, R. O., Tabulated values of cavitation B-factor for helium, H_2, N_2, F_2, O_2, refrigerant 114, and H_2O, Nat. Bur. Stand. (U. S.), Tech. Note 397 (Feb. 1971).

24. Strobridge, T. R., The thermodynamic properties of nitrogen from 64 to 300°K between 0.1 and 200 atmospheres, Nat. Bur. Stand. (U. S.), Tech. Note 129 (Jan. 1962). See also Jacobsen, R. T., Stewart, R. B., McCarty, R. D., and Hanley, H. J. M., Thermophysical properties of nitrogen from the fusion line to 3500 R (1944 K) for pressures to 150,000 psia (10342×10^5 N/m^2), Nat. Bur. Stand. (U. S.) Tech. Note 648 (Dec. 1973).

25. Roder, H. M., Weber, L. A., and Goodwin, R. D., Thermodynamic and related properties of parahydrogen from the triple point to 100°K at pressures to 340 atmospheres, Nat. Bur. Stand. (U. S.), Monogr. 94, (Aug. 1965).

26. ASME Steam Tables, Second Edition, pp. 83-88 (The American Society of Mechanical Engineers, 345 East 47th St. , New York, N. Y. , 1967).

27. Thermodynamic Properties of Refrigerants, pp. 76-101 (American Society of Heating, Refrigerating and Air-Conditioning Engineers, Inc. , 345 East 47th St. , New York, N. Y. , 1969).

28. Billet, M. L. , Thermodynamic effects on developed cavitation in water and freon-113 (M. S. Thesis, Pennsylvania State Univ. , Dept. of Aerospace Engr. , University Park, Pa. , Mar. 1970).

29. Rouse, H. , and McNown, J. S. , Cavitation and pressure distribution on head forms at zero angle of yaw, State Univ. of Iowa, Bulletin 32 (Aug. 1948).

30. Miller, M. J. , and Soltis, R. F. , Visual observations of flow through a radial-bladed centrifugal impeller, color film serial C-256, available on loan from Lewis Research Center, Photographic Branch, Mail Stop 5-2, 21000 Brookpark Road, Cleveland, Ohio 44135.

31. Urasek, D. C. , Investigation of flow range and stability of three inducer-impeller pump combinations operating in liquid hydrogen, NASA TM X-1727 (Jan. 1969).

32. Miller, M. J. , and Soltis, R. F. , Detailed performance of a radial-bladed centrifugal pump impeller in water, NASA Tech. Note D-4613 (June 1968).

33. Moore, R. D. , personal communication to the author.

34. Moore, R. D. , and Meng, P. R. , Cavitation performance of line-mounted 80. 6° helical inducer in hydrogen, NASA TM X-1854 (Aug. 1969). See also Meng, P. R. , and Moore, R. D. , Cavitation performance of 80. 6° helical inducer in liquid hydrogen, NASA TM X-1808 (June 1969).

35. Meng, P. R., Change in inducer net positive suction head requirement with flow coefficient in low temperature hydrogen (27.9° to 36.6° R), NASA Tech. Note D-4423 (Mar. 1968).

36. Meng, P. R., and Moore, R. D., Cavitating and noncavitating performance of 78° helical inducer in hydrogen, NASA TM X-2131 (Nov. 1970).

37. Sengers, J. M. H. L., and Greer, S. C., Thermodynamic anomalies near the critical point of steam, Int. J. of Heat and Mass Transfer 15, 1865-1886, (Pergamon Press, London, 1972).

38. Stimson, H. F., Some precise measurements of the vapor pressure of water in the range from 25 to 100°C, J. Res. Nat. Bur. Stand. (U.S.), 73A (Phys. and Chem.), No. 5, 493-496 (Sept. - Oct. 1969).

39. McCarty, R. D., Thermophysical properties of Helium-4 from 4 to 3000 R with pressures to 15000 PSIA, Nat. Bur. Stand. (U.S.), Tech. Note 622 (Sept. 1972).

40. Prydz, Rolf, and Straty, G. C., The thermodynamic properties of compressed gaseous and liquid fluorine, Nat. Bur. Stand. (U.S.), Tech. Note 392 (Oct. 1970).

41. Weber, L. A., P-V-T, Thermodynamic and related properties of oxygen from the triple point to 300 K at pressures to 33 MN/m^2, J. Res. Nat. Bur. Stand. (U.S.), 74A (Phys. and Chem.), No. 1, 93-129 (Jan. - Feb. 1970). See also McCarty, R. D., and Weber, L. A., Thermophysical properties of oxygen from the freezing liquid line to 600 R for pressures to 5000 psia, Nat. Bur. Stand. (U.S.), Tech. Note 384 (July 1971).

42. Gosman, A. L., McCarty, R. D., and Hust, J. G., Thermodynamic properties of argon from the triple point to 300 K at pressures to 1000 atmospheres, Nat. Bur. Stand. (U.S.), NSRDS-NBS 27 (Mar. 1969).

43. McCarty, R. D., and Weber, L. A., Thermophysical properties of parahydrogen from the freezing liquid line to 5000 R for pressures to 10,000 psia, Nat. Bur. Stand. (U.S.), Tech. Note 617 (April 1972).

44. Esel'son, B. N., Blagoi, Yu. P., Grigor'ev, V. N., Manzhelii, V. G., Mikhailenko, S. A., and Neklyudov, N. P., Properties of liquid and solid hydrogen (translated from Russian, 1971), available from U. S. Dept. of Commerce, Nat. Tech. Inform. Service, Springfield, Va., 22151.

45. Jakobsen, J. K., Liquid rocket engine turbopump inducers, NASA SP-8052 (May 1971).

46. Moore, R. D., Ruggeri, R. S., and Gelder, T. F., Effects of wall pressure distribution and liquid temperature on incipient cavitation of Freon-114 and water in venturi flow, NASA Tech. Note D-4340 (Jan. 1968).

47. Stockman, N. O., and Lieblein, S., Theoretical analysis of flow in VTOL lift fan inlets without crossflow, NASA Tech. Note D-5065 (Feb. 1969).

48. Smith, A. M. O., and Pierce, J., Exact solution of the Neumann Problem. Calculation of non-circulatory plane and axially symmetric flows about or within arbitrary boundaries, Douglas Aircraft Co., Inc., Rept. ES-26988 (Apr. 1958).

49. Katsanis, T., and McNally, W. D., Fortran program for calculating velocities and streamlines on a blade-to-blade stream surface of a tandem blade turbomachine, NASA Tech. Note D-5044 (Mar. 1969).

50. Katsanis, T., and McNally, W. D., Fortran program for calculating velocities in a magnified region on a blade-to-blade stream surface of a tandem blade turbomachine, NASA Tech. Note D-5091 (April 1969).

51. Hamrick, J. J., Ginsburg, A., and Osborn, W. M., Method of analysis for compressible flow through mixed flow centrifugal impellers of arbitrary design, NACA Tech. Rept. 1082 (1952).

52. Abbott, I. H., von Doenhoff, A. E., and Stivers, L. S., Jr., Summary of airfoil data, NACA Tech. Rept. 824 (1945).

53. Abbott, I. H., and von Doenhoff, A. E., Theory of Wing Sections (including a summary of airfoil data), (Dover Publications, New York, N. Y., 1959).

APPENDIX A: Examples of NPSH Prediction Calculations †

Examples of the calculational procedure for predicting NPSH requirements of cavitating impellers and inducers are given. For convenience, eqs (4-14) and (4-16) are repeated below:

$$
\left\{
\begin{array}{l}
\dfrac{(1+K_{c,min})}{(1+K_{c,min})_{ref}} \left(\dfrac{\phi ND_t}{(\phi ND_t)_{ref}}\right)^2 = \dfrac{(NPSH+\Delta h_v)}{(NPSH+\Delta h_v)_{ref}} \\[3em]
\dfrac{B}{B_{ref}} = \left(\dfrac{\alpha_{ref}}{\alpha}\right)^{1.0} \left(\dfrac{\phi ND_t}{(\phi ND_t)_{ref}}\right)^{0.8} \left(\dfrac{\ell/D_t}{(\ell/D_t)_{ref}}\right)^{0.3} \left(\dfrac{D_t}{D_{t,ref}}\right)^{0.9}
\end{array}
\right\}
\tag{4-14}
$$

$$
\left\{
\begin{array}{l}
\dfrac{(1+K_{c,min})}{(1+K_{c,min})_{ref}} \left(\dfrac{\phi ND_t}{(\phi ND_t)_{ref}}\right)^2 = \dfrac{(NPSH+\Delta h_v)}{(NPSH+\Delta h_v)_{ref}} \\[3em]
\dfrac{B}{B_{ref}} = \left(\dfrac{MTWO}{MTWO_{ref}}\right)^{0.51} \left(\dfrac{\ell/D_t}{(\ell/D_t)_{ref}}\right)^{0.28} \left(\dfrac{D_t}{D_{t,ref}}\right)^{0.71}
\end{array}
\right\} .
\tag{4-16}
$$

Lacking cavity length data, the ℓ/D_t ratios in eqs (4-14) and (4-16) are taken as unity--see discussion in section 4.6.

The definitions of BFLASH and MTWO are also given as

$$
B = BFLASH = \left(\dfrac{\rho_\ell}{\rho_v}\right)\dfrac{s_{f1}-s_{f2}}{s_{v2}-s_{f1}} ,
\tag{A-1}
$$

$$
MTWO = \dfrac{V_o}{a_\ell} \left\{\dfrac{1 + B(\rho_\ell/\rho_v)(a_\ell/a_v)^2}{1 + B(\rho_v/\rho_\ell)}\right\}^{0.5} .
\tag{A-2}
$$

† Numerical examples in this Appendix were supplied from the computer computations performed by William R. Parrish.

Computational Procedure

Predicting pump cavitation performance using eqs (4-14) and (4-16) requires two steps. First, from existing pump cavitation data, calculate reference parameters. Then, it is simple to predict a NPSH at different conditions as long as ψ' is held constant.

Reference Parameter Calculation: For example, say that we want to use eq (4-16) to predict NPSH. It is assumed that $K_{c,min}$ is some function of ϕ and ψ' for each impeller and inducer. Two experimental data points are required to calculate reference parameters--at least one of these data points must exhibit measurable 'head depression', Δh_v. This criterion virtually excludes the use of cold water as test fluid for more than one test point. For each pump we may choose two data points at the same values of ϕ and ψ'--under these conditions eqs (4-16) simplify to

$$\left(\frac{N}{N_{ref}}\right)^2 = \frac{NPSH + \Delta h_v}{\left(NPSH + \Delta h_v\right)_{ref}}$$
(A-3a)

and,

$$\frac{B}{B_{ref}} = \left(\frac{MTWO}{MTWO_{ref}}\right)^{0.51}.$$
(A-3b)

There are six unknowns: Δh_v, $(\Delta h_v)_{ref}$, B, B_{ref}, $MTWO$, and $MTWO_{ref}$. The relationships between Δh_v and B, and between B and $MTWO$ are nonlinear and vary with fluid, fluid inlet temperature and inlet velocity. However, these nonlinear relationships can be linearly interpolated over sufficiently short increments of B.

The computational procedure is as follows:

1) Guess a value of $(\Delta h_v)_{ref}$ and determine a corresponding value of B_{ref} from an appropriate table or graph [23]. Equation (A-1) may be used to compute B_{ref} directly using a temperature-entropy diagram for the appropriate fluid.

2) Calculate Δh_v from eq (A-3a).

3) By iteration, compute the correct values of B and MTWO satisfying eq (A-3b).

4) Interpolate [23] the value of Δh_v corresponding to the B found in step 3.

5) Compare the values of Δh_v calculated in steps 2 and 4. If they are equal the correct value of $(\Delta h_v)_{ref}$ has been chosen, otherwise choose another value of $(\Delta h_v)_{ref}$ and return to step 1.

The difference in the calculated values of Δh_v in steps 2 and 4 is nearly linear in $(\Delta h_v)_{ref}$. Therefore, linear extrapolation or interpolation to zero difference is a good guide to choosing the next value of $(\Delta h_v)_{ref}$. Similarly, in step 3 the difference between the left and right sides of eq (A-3b) vs B is nearly linear; therefore, improved guesses for B can be made in the same way as described for $(\Delta h_v)_{ref}$.

Predicting Pump Performance: With reference parameters known, predicting pump cavitation performance for another fluid, fluid temperature, rotative speed, flow condition, or pump geometry at the same value of ψ' is straight-forward. B is computed from the second equation of (4-16) by iteration as described in step 3. The corresponding value of Δh_v is then determined as in step 4, and substituted into the first equation of (4-16). Assuming that $K_{c,min}$ and $(K_{c,min})_{ref}$ are known, the first equation of (4-16) is then used to

solve for the desired (predicted) NPSH. An example illustrating the above procedure is included at the end of this appendix.

Data Reduction: Determining which equation set works best involves the following procedure:

1)   The pump data were divided into sets by holding pump geometry, speed (inducer data only), ϕ, and ψ' constant. The head depressions for two data points are then calculated using the procedure previously outlined in this appendix. Using these calculated values of head depression, the corresponding values of $K_{c,min}$ and S_c are calculated from their definitions. Repeat this procedure for all possible pairs of data points within the data set. Arithmetically average the calculated values of $K_{c,min}$ and S_c and assign the average values to each data point in the data set. $K_{c,min}$ vs ϕ and/or S_c vs ϕ have thus been determined.

2)   Sequentially use all possible combinations of pairs of data points to determine reference data for each pump geometry and value of ψ'. Use each pair of reference data points to predict NPSH for all other data points for all other pump geometries at the chosen value of ψ'. Finally, tabulate the average error in predicting NPSH for each geometry and ψ'.

This procedure is applied to each set of predictive equations to find the set which gives the lowest mean percent error (MPE) in predicted NPSH for each pump geometry, e. g. , the equation set giving the lowest MPE when predicting NPSH values for the impellers and inducer B using inducer A for reference data.

Numerical Example

As an example of how to use the MTWO equations, we will predict the required NPSH for inducer B using reference data from impeller A.

The equations are based on a constant ψ' and the inducer data are at $\psi' = 0.7$--so choose data points 7 and 8 (table 4.3) to obtain reference parameters for predictive purposes.

Calculation of Reference Data: To use the MTWO equations, reference values for B, MTWO, and Δh_v are required. If $K_{c,min}$ is known $(\Delta h_v)_{ref}$ can be calculated from the definition of $K_{c,min}$; however, it is assumed that $K_{c,min}$ is unknown for this part of the example. By choosing data points 7 and 8 (ϕ = constant) we may use eqs (A-3) to evaluate the reference parameters. These simplifications do not alter the method of solution because the remaining terms in eqs (4-16) produce ratios of unity under the prescribed conditions. By calling data point 7 the reference point, eq (A-3a) becomes

$$\frac{29.6 + \Delta h_v}{\left(21.3 + \Delta h_v\right)_{ref}} = \left(\frac{27\ 600}{25\ 000}\right)^2 = 1.2188 . \tag{A-4}$$

As a first guess, assume $(\Delta h_v)_{ref} = 30.0$ m of liquid hydrogen. From (A-4) Δh_v is 32.92 m. This value will be compared with Δh_v found from the B-factor equation--the B for the test point must be found from eq (A-3b). Calculate B for the reference data point using eq (A-1). For $(\Delta h_v)_{ref} = 30.0$ m the BFLASH is 0.8185. With B known, MTWO as calculated from eq (A-2) is 0.3817. Then eq (A-3b) can be written as

$$\frac{B}{0.8185} = \left(\frac{MTWO}{0.3817}\right)^{0.51} \tag{A-5}$$

95

In principle, eq (A-5) can be uniquely solved using the definition of MTWO; however, it is easier to guess a value of B, calculate MTWO and test this value of MTWO in eq (A-5). As a first guess, assume B = 0.83--the corresponding value of MTWO is 0.426. Putting this value into eq (A-5), $B = 0.8185\left(\dfrac{0.4260}{0.3817}\right)^{0.51} = 0.865$. Comparing the assumed and calculated values, the initial guess of B was too small. Now guess B = 0.942, then MTWO = 0.4578 and $B = 0.8185\left(\dfrac{0.4578}{0.3817}\right)^{0.51}$ = 0.898. This time the assumed value is too large; try B = 0.878. This corresponds to MTWO = 0.4392 and $B = 0.8185\left(\dfrac{0.4392}{0.3817}\right)^{0.51}$ = 0.879; this calculated value of B is close enough to the assumed value of 0.878.

This value of B implies a head depression, via eq (A-1),of 31.76 m which is smaller than the 32.92 m calculated from eq (A-4). Therefore, the assumed value of $(\Delta h_v)_{ref}$ was too high; now try $(\Delta h_v)_{ref}$ = 20.0 m. From eq (A-4) Δh_v is 20.815 . B-factor for the reference point is 0.5035 and $(MTWO)_{ref}$ is 0.2893. Repeating the same iterative procedure described above, B-factor for the test point is 0.5405, MTWO is 0.3325 and Δh_v is 21.271 m. This time the head depression calculated from eq (A-1) is larger than the value calculated from eq (A-4).

The next guess of $\Delta h_{v\,ref}$ is found, by linearly interpolating to zero difference in calculated head depression, to be 22.68 m. From eq (A-4) Δh_v is 24.00 m. The B-factor for the reference point is 0.5830 and $(MTWO)_{ref}$ is 0.3140. Solving eq (A-3b) by iteration gives a B-factor for the test point of 0.6260 which corresponds to an MTWO of 0.3611 and Δh_v of 24.11 m. Therefore, the correct value of $(\Delta h_v)_{ref}$ is 22.68 m, $(B)_{ref}$ = 0.5830 and $(MTWO)_{ref}$ = 0.3140.

To obtain reference values for eqs (4-14), the procedure is the same as above except that no iterative procedure is required to calculate the test point B-factor.

Prediction of NPSH at Different Rotative Speed, Temperature,
Flow Coefficient, and Pump Geometry: Using the reference data,
predict the required NPSH for inducer data point 54. It is assumed
that $K_{c,min}$ is known (or can be estimated) for the reference point and
test point. Referring to table 4.3, eqs (4-16) become, for this problem,

$$\left(\frac{1.0 + 3.038}{1.0 + 1.402}\right)\left(\frac{0.110 \,(30000)12.65}{0.225 \,(25000) \,6.78}\right)^2 = \frac{NPSH + \Delta h_v}{(21.3 + 22.68)},$$

or

$$NPSH + \Delta h_v = 88.58 \text{ m;} \qquad (A-6a)$$

$$\frac{B}{0.5830} = \left(\frac{MTWO}{0.3140}\right)^{0.51}\left(\frac{12.65}{6.78}\right)^{0.71},$$

or

$$B = 1.6389 \,(MTWO)^{0.51}. \qquad (A-6b)$$

First eq (A-6b) must be solved by iteration as previously described.
Guess B to be 1.31; this requires that MTWO = 0.7229 for this test point.
Then $B = 1.6389 \,(.7229)^{0.51} = 1.389$, which means the guessed value
is too low. Try B = 1.458, which gives an MTWO = 0.7708 and
$B = 1.6389 \,(0.7708)^{0.51} = 1.435$; this value implies that the guessed
value is slightly too high. Now try B = 1.424 and correspondingly
MTWO = 0.7597, then $B = 1.6389 \,(0.7597)^{0.51} = 1.424$; this is the correct
value and corresponds to a Δh_v of 21.15 m. From eq (A-6a) NPSH
= 88.58 - 21.15 = 67.43 m. From table 4.3 the experimental NPSH
is 67.0 m.

Again, if eqs (4-14) are used, the procedure is identical to the
one just described except that no iterative scheme is required to
calculate the B-factor.

The procedure described and illustrated herein may be applied to any pump geometry, fluid, fluid temperature, rotative speed, flow conditions, etc., as long as ψ' is held constant and appropriate values of $K_{c,min}$ (or S_c) can be estimated. If pump geometry, ψ', and ϕ are held constant, $K_{c,min}$ (or S_c) may be assumed constant and eliminated from the correlative-predictive expressions, i.e., in eqs (4-14) and (4-16).